The intestinal metal transporter ZIP14 maintains systemic manganese homeostasis

Ivo Florin Scheiber, Yuze Wu, Shannon Elizabeth Morgan and Ningning Zhao*

From the Department of Nutritional Sciences, The University of Arizona, Tucson, AZ 85721, USA

Running title: *ZIP14 knock-out enhances Mn absorption*

*To whom correspondence should be addressed: Ningning Zhao, Department of Nutritional Sciences, The University of Arizona, Tucson, AZ 85721, USA. Tel.: (520) 621-9744; Fax: (520) 621-9446; Email: zhaonn@email.arizona.edu.

Keywords: manganese, ZIP14, solute carrier family 39 member 14 (*SLC39A14*), CaCo-2, intestine, metal transporter, ion absorption, metal homeostasis, hypermanganesemia, enterocyte

ABSTRACT

ZIP14 (encoded by the solute carrier 39 family member 14 [*SLC39A14*] gene) is a manganese (Mn) transporter that is abundantly expressed in the liver and small intestine. Loss-of-function mutations in *SLC39A14* cause severe hypermanganesemia. As the liver is regarded as the main regulatory organ involved in Mn homeostasis, impaired hepatic Mn uptake for subsequent biliary excretion has been proposed as the underlying disease mechanism. However, liver-specific *Zip14* knock-out (KO) mice exhibit decreased Mn only in the liver, and do not develop Mn accumulation in other tissues under normal conditions. This suggests that impaired hepatobiliary excretion is not the primary cause for Mn overload observed in individuals lacking functional ZIP14. We therefore hypothesized that increased intestinal Mn absorption could induce Mn hyperaccumulation when ZIP14 is inactivated. To elucidate the role of ZIP14 in Mn absorption, here we used CaCo-2 transwell cultures as a model system for intestinal epithelia. The generation of a ZIP14-deficient CaCo-2 cell line enabled the identification of ZIP14 as the major transporter mediating basolateral Mn uptake in enterocytes. Lack of ZIP14 severely impaired basolateral-to-apical (secretory) Mn transport and strongly enhanced Mn transport in the apical-to-basolateral (absorptive) direction. Mechanistic studies provided evidence that ZIP14 restricts Mn transport in the absorptive direction via direct basolateral reuptake of freshly absorbed Mn. In support of such function of intestinal ZIP14 *in vivo*, Mn levels in the livers and brains of intestine-specific *Zip14*-KO mice were significantly elevated. Our findings highlight the importance of intestinal ZIP14 in regulating systemic Mn homeostasis.

Mn is an essential nutrient. As a cofactor for several enzymes, it is required for the normal function of several physiologic processes including protein glycosylation, detoxification of superoxide and ammonia, and gluconeogenesis (1,2). Excessive Mn accumulation, however, leads to manganism, whose symptoms resemble those of Parkinson's disease (1). Therefore, Mn homeostasis must be tightly controlled at the systemic and cellular levels.

Systemic Mn homeostasis is maintained by intestinal Mn absorption and hepatobiliary Mn excretion (3-6). Oral exposure is the major source of Mn absorption with about 2-3% of Mn being absorbed from a diet adequate in Mn (7). For dietary Mn intakes that are in the physiologic range, oral Mn absorption appears to be primarily controlled by varying intestinal absorption rates (8). However, biliary Mn elimination becomes the main homeostatic mechanism when intestinal control mechanisms are overwhelmed or bypassed, e.g. by intravenous injection or inhalation exposure.

On a cellular level, the distribution of Mn involves mechanisms for entry and exit as well as specific pathways that ensure intracellular transport and targeting. To date, these mechanisms remain poorly defined. Components of the iron (Fe) metabolic pathways, citrate-, choline-, dopamine-, and calcium-transporters, the sodium-calcium

exchanger as well as the ATPases Park9 and SPCA1 have been implicated in Mn metabolism (9). More recently, spurred by the discovery of human mutations, members of the ZnT- and ZIP-families of metal transporters, namely ZnT10, ZIP8 and ZIP14 have been identified as crucial players in cellular Mn metabolism *in vivo* (10-14).

Previous studies have shown that ZIP14 is capable of mediating the uptake of Mn *in vitro* (15). Highlighting the function of ZIP14 as a Mn transporter *in vivo*, homozygous mutations of *ZIP14* result in Mn hyperaccumulation in the blood and other tissues of affected individuals without apparent effects on other metals (10,16-18). Initially it was postulated that the primary function of ZIP14 is hepatic Mn uptake for subsequent biliary excretion and that the Mn hyperaccumulation observed in other tissues is secondary to the defect of hepatic ZIP14 (10). The latter hypothesis, however, was falsified by experiments involving a liver-specific *Zip14* KO mouse line (19). Specifically, these mice did not display elevated Mn in the blood or other tissues in contrast to global *Zip14* KO mouse models, although ZIP14 has been clearly demonstrated to be required for hepatobiliary Mn excretion under high Mn conditions (19-22).

ZIP14 is also highly abundant in the small intestine of humans and mice (23,24). We hypothesize that, if not impaired hepatobiliary excretion, increased intestinal Mn absorption could be the primary cause for the Mn hyperaccumulation observed in individuals lacking functional ZIP14. To test our hypothesis, we generated a CaCo-2 cell line with *ZIP14* inactivation (CaCo-$2_{\Delta ZIP14}$ cells). Differentiated monolayers of this cell line exhibited a dramatic defect in basolateral Mn uptake. Apical-to-basolateral Mn transport in CaCo-$2_{\Delta ZIP14}$ cells was strongly increased compared to that of wild type CaCo-2 (CaCo-2_{WT}) cells. Further mechanistic studies provided evidence that ZIP14 controls enterocyte Mn absorption by mediating basolateral reuptake of freshly absorbed Mn. To evaluate the physiologic relevance of this novel homeostatic mechanism, we generated intestine-specific *Zip14* KO mice. These mice developed markedly increased Mn levels in their livers and brains. Overall, our results suggest an important function of intestinal ZIP14 in the control of systemic Mn homeostasis.

Results

Generation of a ZIP14 KO CaCo-2 cell line

To assess the function of ZIP14 in enterocytes we inactivated the *ZIP14* gene in CaCo-2 cells via CRISPR/Cas9-mediated gene KO by targeting the start codon in exon 2 of *ZIP14* (Fig. 1A). CaCo-2 cells differentiate spontaneously into polarized enterocytes when grown on permeable filter supports (25). Such CaCo-2 cell cultures provide a well-established model system to study the uptake as well as absorptive (apical-to-basolateral direction) and secretory (basolateral-to-apical direction) fluxes of drugs and nutrients in the intestinal epithelium. This model has been extensively used to study the mechanisms of intestinal Fe-uptake and -transport. In general, results from Fe absorption studies conducted *in vitro* using CaCo-2 cells correlate well with observations made *in vivo* (26), validating the use of the CaCo-2 cell model for studying intestinal metal uptake and transport.

By using the CRISPR/Cas9 approach, we isolated a CaCo-2 cell clone termed CaCo-$2_{\Delta ZIP14}$ with a single base pair insertion at the predicted Cas9-cleavage site (Fig. 1B). This insertion caused a frame shift mutation, yielding a non-functional protein that consists of only 26 amino acids (Fig. 1C). Immunoblot analysis confirmed the inactivation of *ZIP14* in CaCo-$2_{\Delta ZIP14}$ cells (Fig. 1D and Fig. S1).

Characterization of CaCo-2_{WT} and CaCo-$2_{\Delta ZIP14}$ transwell cultures

In order to study Mn transport across the intestinal epithelium and the role of ZIP14 in this process, both CaCo-2_{WT} and CaCo-$2_{\Delta ZIP14}$ cells were grown into differentiated monolayers for at least 21 days. The presence of polarized monolayers was confirmed by confocal microscopy using the tight junction protein ZO-1 as the apical marker and Na^+, K^+-ATPase as the basolateral marker (Fig. 2A). Further analysis of these images revealed diameters of 11 μm and 9 μm and heights of 12 μm and 19 μm for CaCo-2_{WT} cells and CaCo-$2_{\Delta ZIP14}$ cells, respectively. The consequential larger basolateral and apical surface areas and volumes of CaCo-$2_{\Delta ZIP14}$ transwell cultures, which we estimated to be about 180% and 150% of equivalent CaCo-2_{WT} cultures, are mirrored by a similar increase in the protein contents of these cultures

(Fig. 2B). Thus, to compensate for the increased surface, we normalized our uptake- and transport-data to the protein content in the respective transwell insert. The integrity of the monolayers was tested by the Lucifer Yellow (LY) rejection assay. Apparent LY permeability (P_{app}) coefficients below 10 nm x s^{-1} have been reported to be indicative of well-established CaCo-2 monolayers (27). P_{app} coefficients determined for both CaCo-2_{WT} and CaCo-$2_{\Delta ZIP14}$ monolayers fell in that range but were significantly higher in CaCo-$2_{\Delta ZIP14}$ transwell cultures (Fig. 2C). Due to the smaller diameter of CaCo-$2_{\Delta ZIP14}$ cells, CaCo-$2_{\Delta ZIP14}$ transwell cultures possess a greater number of paracellular pores, the sites of paracellular transport, which may partially account for the increased permeability of LY. Consequently, when normalized to protein, P_{app} did not differ significantly between the cultures.

Deletion of *Zip14* in mice does not affect the intestinal contents of Mn, zinc (Zn), Fe and copper (Cu) (19). To test whether this observation is reflected in the CaCo-2-transwell system, we measured their specific contents by inductively coupled plasma mass spectrometry (ICP-MS). We found the specific contents of Mn, Zn and Fe in CaCo-$2_{\Delta ZIP14}$ monolayers to be significantly lower compared to those in CaCo-2_{WT} cells (Fig. 2D). We ascribe this discrepancy to the *in vivo* situation to limitations of our transwell system. *In vivo* enterocytes can acquire nutrients from both the intestinal lumen and the arterial blood. Transporters functioning in metal uptake from the luminal side of the proximal intestine, such as DMT1, are optimally adjusted to the acidic milieu of the intestinal tract (28-30). In the transwell system, however, the pH in the apical chamber is maintained at 7.4 during regular culturing, impairing efficient metal uptake from this side.

To confirm previous results on the localization of ZIP14 in enterocytes (21,31) we studied the localization of ZIP14 in polarized CaCo-2_{WT} monolayers. Basolateral and apical surface proteins were isolated by a biotinylation approach. Immunoblotting for ZIP14 demonstrated the enrichment of ZIP14 at the basolateral membrane of CaCo-2_{WT} cells (Fig. 2E and Fig. S2). This localization of ZIP14 in enterocytes supports a role of ZIP14 in the uptake of Mn from the blood.

ZIP14 is the major transporter responsible for Mn uptake at the basolateral membrane

To establish the function of ZIP14 in the Mn metabolism of enterocytes, we first studied the consequences of *ZIP14* KO on basolateral ^{54}Mn accumulation. If not stated otherwise, during the experiments the extracellular pH was maintained at 6.1 in the apical and 7.4 in the basolateral compartment to mimic the physiologic situation, i.e. the acidic intraluminal pH of the proximal small intestine and the normal blood pH. Upon addition of 0.1 μM ^{54}Mn, which is close to the low Mn concentrations in mammalian serum [0.01 μM - 0.04 μM; (32)] to the basolateral chamber, CaCo-2_{WT} cells rapidly accumulated ^{54}Mn up to 180 minutes after which cellular ^{54}Mn contents had reached a steady state (Fig. 3A). Basolateral ^{54}Mn accumulation by CaCo-$2_{\Delta ZIP14}$ cells was severely compromised, identifying ZIP14 as the primary transporter mediating Mn uptake at the basolateral membrane of CaCo-2 cells. The residual basolateral ^{54}Mn accumulation observed in CaCo-$2_{\Delta ZIP14}$ cells suggests the presence of an alternative, low-capacity entry route for Mn at the basolateral membrane.

Next we examined the pH dependence of basolateral Mn accumulation by measuring the amount of ^{54}Mn accumulated by CaCo-2 cells incubated in media at pH 6.1, pH 6.8 or pH 7.4 for 4 h. These experiments were performed by adjusting the incubation media to the same pH in both the basolateral and apical compartments. Basolateral ^{54}Mn accumulation by CaCo-2_{WT} cells was maximal at pH 7.4 and decreased with decreasing pH (Fig. 3B). While CaCo-2_{WT} cells still accumulated substantial amounts of ^{54}Mn at pH 6.8, the basolateral ^{54}Mn accumulation in these cells decreased by about 90% at pH 6.1. Consistent with ZIP14 being the major transporter mediating Mn uptake at the basolateral membrane of CaCo-2_{WT} cells, similar pH dependencies have been reported for ZIP14-mediated Fe and Zn transport (33,34). Opposite to what we observed for CaCo-2_{WT} cells, basolateral ^{54}Mn accumulation by CaCo-$2_{\Delta ZIP14}$ cells was maximal at pH 6.1 and lower at pH 6.8 and 7.4.

ZIP14 deletion does not substantially affect apical Mn uptake

In contrast to the striking effect of *ZIP14* KO observed for basolateral ^{54}Mn accumulation, ^{54}Mn accumulation from the apical chamber was observed to be rather similar in both cell lines. Within 6 h both CaCo-2_{WT} and CaCo-$2_{\Delta ZIP14}$ cells accumulated about 30 pmol x mg^{-1} ^{54}Mn from the apical chamber (Fig. 3C). While apical ^{54}Mn-accumulation by CaCo-$2_{\Delta ZIP14}$ cells proceeded at slightly faster pace between 30 minutes and 3 h of incubation, ^{54}Mn contents in CaCo-$2_{\Delta ZIP14}$ cells approached a steady state thereafter whereas ^{54}Mn contents in CaCo-2_{WT} cells continued to rise at almost constant speed for up to 6 h. Mn accumulation by CaCo-2 cells is a complex process involving the uptake and export of Mn at the apical side, its intracellular sequestration and transport, as well as its basolateral uptake and export. The accelerated accumulation of ^{54}Mn from the apical side by CaCo-$2_{\Delta ZIP14}$ cells compared to CaCo-2_{WT} cells between 30 minutes and 3 h may therefore be explained by several mechanisms, including a ZIP14-dependent export process of freshly acquired Mn (either at the basolateral or apical side) that is activated when cellular Mn levels rise above a certain threshold.

Apical ^{54}Mn accumulation exhibited the same dependence on the extracellular pH in both CaCo-2_{WT} and CaCo-$2_{\Delta ZIP14}$ cells, being maximal at pH 6.1 and decreasing with increasing pH (Fig. 3D). While this is relevant under physiological conditions as the pH in the proximal intestine is rather acidic, the mechanisms mediating Mn uptake from the intestinal lumen remain unknown. DMT-1, which is strongly expressed at the intestinal brush border (35) and at the apical membrane of CaCo-2 cells (Fig. 2E), had long been regarded as a potential candidate. However, recently Shawki *et al.* (36) reported that DMT-1 is not required for Mn absorption in intestine-specific *Dmt-1* KO mice, contrasting previous observations made in the Belgrade rat model (37,38).

ZIP14 restricts Mn absorption

Having established that ZIP14 is the major transporter mediating basolateral Mn uptake and that ZIP14 deletion does not substantially affect Mn uptake from the apical membrane of CaCo-2 cells, we next investigated the transport of Mn across CaCo-2 cell monolayers in both basolateral-to-apical and apical-to-basolateral directions. Upon application of 0.1 μM ^{54}Mn to the basolateral side of CaCo-2_{WT} cells, the amounts of ^{54}Mn detected in the apical chamber rapidly increased with time (Fig. 4A). Following an exponential phase that lasted about 90 minutes, the amounts of ^{54}Mn on the apical side increased almost linearly for up to 240 minutes. In contrast, CaCo-$2_{\Delta ZIP14}$ cells transported only minimal amounts of ^{54}Mn from the basolateral to apical compartment within 240 minutes. This result could be expected since CaCo-$2_{\Delta ZIP14}$ cells lack substantial basolateral Mn uptake activity.

After addition of 0.1 μM ^{54}Mn to the apical chamber to initiate the apical-to-basolateral transport, we observed a slow, exponential rise in the amounts of ^{54}Mn detected in the apical chamber in the first 150 minutes followed by a linear increase for up to 240 minutes for CaCo-2_{WT} cells (Fig. 4B). The time dependence of apical-to-basolateral Mn transport by CaCo-$2_{\Delta ZIP14}$ cells displayed a similar pattern but with significantly higher amounts of ^{54}Mn accumulated in the basolateral compartment. The increased apical-to-basolateral Mn transport by CaCo-$2_{\Delta ZIP14}$ cells compared to CaCo2_{WT} cells strongly suggests that intestinal ZIP14 is required to restrict Mn absorption.

ZIP14 has been described as a broad-scope metal transporter, capable of mediating the cellular uptake of several metals including Fe (33,34). Hence, we tested the consequences of ZIP14 deletion on Fe accumulation and transport in CaCo-2 cell monolayers upon addition of 1 μM $^{59}Fe^{2+}$ or $^{59}Fe^{3+}$. Consistent with the function of ZIP14 as a Fe^{2+}-transporter, basolateral $^{59}Fe^{2+}$ accumulation was lowered by 30% in CaCo-$2_{\Delta ZIP14}$ cells, whereas $^{59}Fe^{3+}$ accumulation did not differ significantly from CaCo-2_{WT} cells (Fig. S3A). In contrast to Mn transport, the lack of ZIP14 did not affect the apical-to-basolateral transport of $^{59}Fe^{2+}$ and $^{59}Fe^{3+}$ (Fig. S3C, D), most likely since Fe is released from the cells into the media in its ferric state. This result suggests that in the CaCo-2 transwell system, functional ZIP14 specifically restricts Mn absorption.

ZIP14 mediates Mn reuptake from the basolateral membrane to restrict Mn absorption

In CaCo-2 cells, ZIP14 restricts the flux of Mn in the absorptive direction (Fig. 4B), but how is it accomplished? ZIP14 is localized to the basolateral

membrane of CaCo-2 cells (Fig. 2E) and is required for efficient Mn uptake from the basolateral side (Fig. 3A, B). Accordingly, direct reuptake of freshly absorbed Mn is a plausible mechanism by which ZIP14 may restrict Mn absorption. If so, inhibiting basolateral Mn uptake should increase apical-to-basolateral Mn transport in CaCo-2_{WT} cells, but not in CaCo-$2_{\Delta ZIP14}$ cells. We used three approaches to minimize basolateral Mn reuptake.

First, since ZIP14-mediated ^{54}Mn uptake is highest at pH 7.4 and decreases by 95% at pH 6.1 (Fig. 3B), we studied the transport of 0.1 μM ^{54}Mn from the apical to basolateral compartment with the pH in the basolateral chamber being maintained at pH 7.4 as the normal condition or adjusted to pH 6.1. For CaCo-2_{WT} cells ^{54}Mn accumulation in the basolateral chamber was found to be about five times higher at a basolateral pH of 6.1 compared to a basolateral pH of 7.4 (Fig. 5A). In contrast, apical-to-basolateral Mn transport by CaCo-$2_{\Delta ZIP14}$ cells slightly decreased with lowering the basolateral pH from pH 7.4 to pH 6.1 (Fig. 5B). These observations are consistent with the pH dependence of basolateral Mn accumulation (Fig. 3B), and suggest that Mn transport in the apical-to-basolateral direction is limited by basolateral Mn uptake.

Apical-to-basolateral Mn transport requires about 150 minutes to become fully established (Fig. 4B). To exclude that the modulation of basolateral mediated Mn uptake by altering the basolateral pH induces changes in the recruitment of transporters required for the export of intracellular Mn at the basolateral side, we removed ^{54}Mn from the apical compartment after 4 h of ^{54}Mn preloading and followed ^{54}Mn accumulation in the basolateral compartment for another 3 h, with the pH of the basolateral compartment either maintained at the same pH as in the first 4 h, or switched to pH 6.1 or pH 7.4 (Fig. 5C, D, E, F). Alteration of the basolateral pH caused a rapid response in the apical-to-basolateral transport rates. The immediate effect of the basolateral pH switch on the apical-to-basolateral Mn transport in CaCo-2 cells, suggests that the elevated Mn absorption at lower pH observed in CaCo-2_{WT} cells is indeed due to impaired ZIP14 mediated Mn uptake at low pH rather than due to alterations in transporter abundance at the basolateral membrane.

Second, we used excess Zn to compete with ^{54}Mn reuptake from the basolateral chamber. Zn has previously been reported as a potent competitive inhibitor of ZIP14-mediated Mn uptake (33). However, initial experiments revealed that a ten-times excess of Zn does not inhibit basolateral ^{54}Mn accumulation by CaCo-2_{WT} cells when Dulbecco's modified Eagles medium (DMEM) was used as the experimental medium (Fig. S4A). In contrast, when salt-based incubation buffer was used instead of DMEM, excess Zn strongly impaired basolateral ^{54}Mn accumulation in CaCo-2_{WT} cells (Fig. S4B). Thus, to study the effect of Zn on apical-to-basolateral transport CaCo-2 monolayers were first loaded for 4 h with 0.1 μM ^{54}Mn from the apical side, after which the accumulation of ^{54}Mn in the basolateral compartment was followed for 90 minutes using salt-based incubation buffer with or without 2 μM Zn. The presence of 2 μM Zn strongly enhanced ^{54}Mn accumulation in the basolateral compartment of CaCo-2_{WT} transwell cultures (Fig. 6A), suggesting that Zn impairs the direct reuptake of freshly absorbed Mn by competing with ^{54}Mn for uptake via ZIP14. Consistent with this view, ^{54}Mn accumulation in the basolateral compartment of CaCo-$2_{\Delta ZIP14}$ transwell cultures (Fig. 6B) was not altered by Zn.

Third, we sought to prevent ZIP14-mediated Mn reuptake by chelating freshly absorbed Mn with EDTA or desferrioxamine (DFO), which are strong chelators for Mn(II) and Mn(III), respectively (39,40). Since both EDTA and DFO are membrane impermeable (41), the intracellular Mn trafficking would not be disturbed. To carry out the experiment, CaCo-2 monolayers were first loaded for 4 h with 0.1 μM ^{54}Mn from the apical side, after which the accumulation of ^{54}Mn in the basolateral compartment was followed for 90 minutes using salt-based incubation buffer containing either no chelator, 100 μM $CaNa_2EDTA$ or 1 mM DFO. The presence of both EDTA or DFO caused an increased accumulation of ^{54}Mn in the basolateral compartment of CaCo-2_{WT} transwell cultures (Fig. 6C and E) but not in CaCo-$2_{\Delta ZIP14}$ transwell cultures (Fig. 6D and F). As Mn is released close to the plasma membrane, the moderate effect of both chelators on the accumulation of ^{54}Mn in the basolateral compartment of CaCo-2_{WT} transwell cultures is most likely due to limited access of EDTA and DFO to Mn prior to its reuptake. Nevertheless, these results further support our proposed mechanism that ZIP14 restricts Mn

absorption by direct reuptake of freshly absorbed Mn.

Intestine-specific deletion of Zip14 in mice leads to Mn overload

To test the physiologic relevance of our findings, we generated mice carrying *Zip14* conditional alleles (*Zip14*$^{flox/flox}$ mice) by flanking exon 3 and 4 of the *Zip14* with *loxP* sites (Fig. 7A). The correct insertion of *loxP* sites was verified by genotyping (Fig. 7B). We then generated intestine-specific *Zip14* KO mice by crossing *Zip14*$^{flox/flox}$ mice with *Vil-Cre* mice. For comparison, we also generated liver-specific *Zip14* KO mice. Tissue-specific inactivation of *Zip14* was confirmed by immunoblot analysis (Fig. 7C and Fig. S5).

We used ICP-MS to determine Mn levels in whole blood, livers and brains from *Zip14*$^{flox/flox}$ mice, intestine-specific, and liver-specific *Zip14* KO mice at three weeks of age. We observed a clear difference in the hepatic Mn levels from liver-specific *Zip14* KO mice and intestine-specific *Zip14* KO mice (Fig. 7D): consistent with previous results (19), hepatic Mn contents were significantly reduced in liver-specific *Zip14* KO mice; in contrast, Mn levels in livers from intestine-specific *Zip14* KO mice were more than two times that of controls, revealing that loss of ZIP14 in the intestine increases body Mn burden. This observation establishes the importance of the intestinal ZIP14 in the control of systemic Mn homeostasis, and is in full agreement with our discovery that deletion of ZIP14 in CaCo-2 cells results in increased apical-to-basolateral Mn transport.

Although Mn concentrations in the blood of intestine-specific *Zip14* KO mice did not increase (Fig. 7D), brain Mn contents were double that of control and liver-specific *Zip14* KO mice at three-week old. An explanation could be that Mn homeostasis can still be regulated through hepatobiliary excretion in intestine-specific *Zip14* KO mice, but the liver cannot clear all of the excess Mn entering the portal blood, and elevated Mn entering the systemic circulation are readily absorbed by other tissues, including the brain. Further studies are required to evaluate the Mn contents in other tissues of intestine-specific *Zip14* KO mice and to examine the consequences of *Zip14* deletion in both the liver and intestine.

Discussion

In the present study, we identified ZIP14 as the major transporter mediating basolateral Mn uptake in enterocytes. Moreover, we provide *in vitro* and *in vivo* evidence that this function of ZIP14 is required for the control of Mn homeostasis.

CaCo-2 cell cultures provide a well-established model system to study the uptake as well as absorptive and secretory fluxes of drugs and nutrients in the intestinal epithelium (25). Genetically modified Caco-2 cell lines have previously been used to study the uptake and transport of metals. Just recently, a stable CaCo-2 cell line over-expressing ZnT10 has been employed to prove the ability of this transporter to mediate the efflux of cellular Mn at the apical membrane (52). RNA interference (RNAi)-mediated gene knockdown has been used to study the functions of ZnT1, ferroportin and DMT1 in CaCo-2 cell monolayers (42,43). A drawback of RNAi-mediated gene knock-down is the possibility of residual gene expression that may mask potential phenotypes, a complication that we avoided by generating a *ZIP14* KO CaCo-2 cell line using the CRISPR/Cas9 system.

In contrast to previous studies investigating Mn uptake and Mn transport by CaCo-2 cells (44-46), we maintained a pH of 6.1 in the apical and a pH of 7.4 in the basolateral compartment to mimic the physiologic situation. Such pH gradient is routinely used in studies investigating Fe uptake and Fe transport in CaCo-2 cells, and is of uttermost importance when studying apical Mn uptake and apical-to-basolateral Mn transport as substantial Mn transport in the absorptive direction occurs only at acidic apical pH (Fig. S6). To account for the low Mn concentrations in mammalian serum [0.01 μM - 0.04 μM; (32)], breast milk [0.004 μM - 0.55 μM; (47)] and infant formulas[0.73 μM - 20 μM; (48)] we used a concentration of 0.1 μM Mn as our standard concentration, whereas non-physiologic high Mn concentrations of 30 μM to 146 μM were employed in the previous studies (44-46).

Systemic Mn homeostasis is maintained by the regulation of both intestinal Mn absorption and hepatobiliary Mn excretion (3-6). The accumulation of excess Mn in blood and several organs in individuals with homozygous mutations in *ZIP14* (10,16-18) and global *Zip14* KO mice (19-22) indicates a crucial requirement of ZIP14 in

systemic Mn homeostasis. ZIP14 has convincingly been shown to mediate hepatobiliary Mn excretion in concert with ZnT10 (20). However, in contrast to the global *Zip14* KO mice, liver-specific *Zip14* KO mice do not hyperaccumulate Mn (19), indicating that ZIP14 is involved in extrahepatic processes required for the maintenance of systemic Mn homeostasis.

In the present study, we identified ZIP14 as the primary transporter mediating efficient Mn uptake from the basolateral side of enterocytes. This function of ZIP14 is consistent with its localization in the intestine and CaCo-2 monolayers (21,31), and the reported pH dependencies of ZIP14-mediated Fe and Zn uptake (33,34). Our results also indicate that CaCo-2 cells possess alternative systems to acquire Mn from the basolateral compartment that become evident in $CaCo2_{\Delta ZIP14}$ cultures, however, due to the low capacity, these mechanisms are unlikely to compensate for the loss of ZIP14 function *in vivo*.

Apical Mn uptake does not differ substantially in $CaCo\text{-}2_{WT}$ and $CaCo2_{\Delta ZIP14}$ cultures, but *ZIP14* inactivation strongly enhances the flux of Mn in the absorptive direction, suggesting that functional ZIP14 is required to limit Mn absorption. Mechanistically, we demonstrate that inhibiting ZIP14-mediated basolateral Mn uptake by lowering the basolateral pH, Zn competition, and chelation of freshly absorbed Mn all increases Mn transport in the absorptive direction. These observations strongly support that intestinal ZIP14 contributes to the maintenance of systemic Mn homeostasis by restricting dietary Mn absorption via direct reuptake of freshly absorbed Mn. Such function of intestinal ZIP14 would not only explain the Mn hyperaccumulation observed in individuals lacking functional ZIP14 but also the lack of Mn accumulation in the liver-specific *Zip14* KO mice.

Providing evidence that ZIP14 restricts dietary Mn absorption *in vivo*, intestine-specific *Zip14* KO mice display elevated Mn contents in the liver and brain, indicating that enterocyte specific KO of *Zip14* causes Mn overload. However, these mice do not develop increased blood Mn concentrations at three weeks of age since the liver control system is still in place and excess Mn is likely to be cleared from the blood by extrahepatic tissues, including the brain.

In summary, we show that ZIP14 is crucial for efficient Mn uptake from the basolateral membrane of enterocytes. We provide evidence that one potential mechanism by which ZIP14 restricts Mn absorption and limits whole body Mn burden is through direct reuptake of freshly absorbed Mn. Moreover, our *in vivo* data provides strong evidence that intestinal ZIP14 plays an important role in maintaining systemic Mn homeostasis.

Experimental procedures

Cell cultures. CaCo-2 (ATCC HTB-37™) cells were maintained in growth medium [80% DMEM containing 1 mM pyruvate (Corning, Corning, NY, USA)] supplemented with 3.7 g x L^{-1} $NaHCO_3$, 1x non-essential amino acids (Thermo Fisher Scientific, Waltham, MA, USA), 100 units x mL^{-1} penicillin, 100 µg x mL^{-1} streptomycin (Thermo Fisher Scientific) and 20% fetal bovine serum (VWR, Radnor, PA, USA) at 37°C and 5% CO_2 in the humified atmosphere of an incubator. The Mn concentration of the growth medium was determined to be 0.056 ± 0.005 µM by ICP-MS as described in the section *ICP-MS analysis of metals* (Fig. S7). The cells were split every three to four days following detachment by treatment with 0.25% trypsin in phosphate-buffered saline (PBS) without calcium and magnesium and containing 0.2% EDTA (Thermo Fisher Scientific). For routine cell culture the cells were seeded in cell culture dishes of 55 cm^2 (Thermo Fisher Scientific) at a density of 0.1 x 10^4 ($CaCo\text{-}2_{WT}$) or 0.14 x 10^4 ($CaCo2_{\Delta ZIP14}$) cells per cm^2. For preparation of CaCo-2 cell monolayers 1 x 10^5 cells per cm^2 were seeded in Transwell-Clear™ inserts with 0.4 µm pore size of 4.67 cm^2 or 1.12 cm^2 surface area (both from Corning) that had been incubated with growth medium for 24 h prior to seeding. Inserts of 4.67 (1.12) cm^2 were placed in 6-well (12-well) plates with 2.6 (1.5) mL of growth medium in the well and 1.5 (0.5) mL in the insert. The growth medium was changed every two to three days. CaCo-2 cell monolayers were used for experiments between 21-27 days after seeding.

Generation of a CaCo-2 ZIP14 KO cell line. The CaCo-2 *ZIP14* KO cell line was generated using the CRISPR-Cas9 system (49). The guide RNA sequence (5′-GTG CAG CAG CAG CAG CTT CA-3′), complementary to a sequence in proximity to the start codon of the *ZIP14* gene, was cloned into the pX330-U6-Chimeric_BB-CBh-hSpCas9 vector (50). CaCo-2 cells were transfected with *ZIP14*-targeting vector using Lipofectamine™

3000 (Thermo Fisher Scientific). Briefly, on the day of the transfection CaCo-2 cells were seeded in 12-well plates (Thermo Fisher Scientific) at a density of 0.2 x 10^4 cell per cm^2 and incubated for 6 h in growth medium without penicillin and streptomycin. The medium was changed to growth medium and the DNA-lipid complex (1 µg plasmid DNA, 2 µL P3000™ reagent, 3 µL Lipofectamine™ 3000 reagent, 95 µL DMEM), prepared 3 h in advance according to the protocol provided by the manufacturer, was added dropwise to the cells. The cells were grown for 72 h after which the medium was changed to growth medium containing 7.5 µg x mL^{-1} puromycine for selection. After 48 h the cells contained in one well were split into four culture dishes of 55 cm^2 and cultured for three weeks in growth medium. Single-cell clones were transferred to 12-well plates for screening by immunoblot analysis with a human ZIP14-specific antibody described in the section *Antibodies*. Cell clones lacking ZIP14 expression were subcloned. *ZIP14* inactivation in selected subclones was confirmed by immunoblot analysis and DNA sequencing.

Animals. All mice were maintained on a NIH-31 irradiated traditional rodent diet (Teklad 7913; Envigo, Indianapolis, IN, USA) and housed in the Laboratory Animal facility at the University of Arizona. Procedures for animal experiments were approved by the Institutional Animal Care and Use Committee. Mice carrying *Zip14* conditional alleles (*Zip14*$^{flox/flox}$ mice) were generated by flanking exon 3 and 4 of *Zip14* gene with *loxP* sites (Cyagen, Santa Clara, CA). The transgenic mice expressing Cre recombinase under the intestine-specific villin promotor (*Vil-Cre* mice) and liver-specific albumin promoter (*Alb-Cre* mice) were purchased from the Jackson Laboratory. All mice are on the C57BL/6 background. Genotyping procedures were performed by using mouse tail snipping and Mouse Direct PCR kit (Bimake, TX, USA). Mice were sacrificed after anaesthetizing with ketamine/xylazine at three weeks of age. Tissues were collected and immediately frozen in liquid nitrogen and stored at -80°C until further analyses.

Antibodies. Since antibodies against mouse ZIP14 (mZIP14) and human ZIP14 (hZIP14) are not commercially available, we employed the approach of expressing glutathione S-transferase (GST) fusion proteins in *E. Coli* to produce and purify the immunogens for the production of antibodies. To construct a vector carrying mZIP14 or hZIP14 fusion protein, the sequence encoding N-terminal serine 31 to proline 146 of mZIP14, or serine 32 to proline 148 of hZIP14 was PCR amplified and cloned into pGEX-3X (Addgene, Watertown, MA, USA) vector using BamHI-ECoRI linkers. The fusion protein was isolated from *E. Coli* and purified by affinity chromatography on Gluthathione-Sepharose 4B (GE Healthcare, Chicago, IL, USA). The immunization procedures were performed by the Pocono Rabbit Farm & Laboratory (Canadensis, PA, USA). The antisera obtained from the test bleeds were analyzed for ZIP14 recognition by immunoblotting. Antisera were cleared by Glutathione Sepharose cross-linked with GST to remove anti-GST antibody. The cleared flow-through fractions were collected and used to purify anti-hZIP14 or anti-mZIP14 antibody using Glutathione Sepharose cross-linked with GST-mZIP14 or GST-hZIP14 fusion protein (Fig. S8).

The rabbit anti-ZO-1 polyclonal antibody (21773-1-AP), rabbit anti-DMT1 polyclonal antibody (20507-1-AP), horseradish peroxidase (HRP)-conjugated mouse anti-beta ACTIN monoclonal antibody (HRP-60008), HRP-conjugated mouse anti-GAPDH monoclonal antibody (HRP-60004), and HRP-conjugated goat anti mouse IgG (H+L) secondary antibody (SA00001-1) were from Proteintech (Rosemont, IL, USA). The monoclonal mouse anti-Na^+, K^+-ATPase α1 antibody (sc-21712) was from Santa Cruz (Dallas, TX, USA). HRP-conjugated goat anti-rabbit IgG (H+L) secondary antibody (65-6120), Alexa Fluor 594-conjugated donkey anti-mouse IgG (H+L) secondary antibody (A21203) and Alexa Fluor 488-conjugated goat anti-rabbit (A21206) secondary antibody were from Thermo Fisher Scientific.

Immunoblot analysis. Cells and mouse tissues were lysed in NETT buffer [150 mM NaCl, 5 mM EDTA, 10 mM Tris, 1% Triton X-100 and 1x protease inhibitor cocktail (Bimake, Houston, TX, USA), pH 7.4]. Nuclei were removed by centrifugation (15000 x g / 4°C / 15 minutes). Protein concentrations of cell lysates were determined using the RC DC™ Protein Assay (Bio-Rad Life Science, Hercules CA, USA). Cell lysates were mixed with 1x Laemmli buffer and incubated for 30 min at 37 °C. Proteins were separated

electrophoretically on an SDS/10% polyacrylamide gel and transferred to nitrocellulose membranes (GVS, Sanford, ME, USA). Following blocking of unspecific binding sites with 5% (w/v) non-fat dry milk in Tris-buffered saline with Tween-20 [TBS-T; 10 mM Tris/HCl, 150 mM NaCl, 0.1% (v/v), 1 mL Tween-20, pH 7.5], membranes were probed at 4 °C overnight with rabbit anti-hZIP14 (1:3000), anti-mZIP14, or anti-DMT1 (1:5000) antibodies in blocking buffer. The membranes were washed four times with TBS-T (5 min each) and subsequently incubated for 1 h at room temperature (RT) with HRP-conjugated goat anti-rabbit secondary antibodies (1:5000). After two washes with TBS-T and TBS (5 min each), blots were developed using enhanced chemiluminescence (SuperSignal West Pico, Thermo Fisher Scientific) and the ChemiDoc™ MP Imaging System (Bio-Rad Life Science). To confirm equivalent loading, blots were stripped for 15 min in Restore PLUS Western Blot Stripping Buffer (Thermo Fisher Scientific), blocked for 1 h in blocking buffer, and reprobed with HRP-conjugated antibodies directed against GAPDH (1:20000) and/or β-ACTIN (1:20000) and. Mouse anti-Na^+, K^+ ATPase (1:3000) followed by HRP-conjugated secondary antibodies (1:5000) served as loading control for plasma membrane proteins. Blots were visualized and quantified using the ChemiDoc MP imaging system with Image Lab software (Bio-Rad).

Isolation of genomic DNA, PCR & Sequencing. Genomic DNA was isolated using the Quick-DNA™ Miniprep Plus Kit (Zymo Research, Irvine, CA, USA) according to the protocol provided by the manufacturer. The guide RNA targeting region in exon 2 of the *ZIP14* gene was amplified with DNA-specific primers (forward primer, 5′-GAG CAG AGA AGC AGA GAC TGA-3′; reverse primer, 5′- ACG GTA AGG CTC CCC TGT-3′). PCR products were isolated by agarose gel electrophoresis and purified with the Wizard SV Gel and PCR Clean-Up System (Promega Corporation, Madison, WI, USA). The purified PCR products were sent for sequencing to MCLAB, San Francisco, CA, USA.

ICP-MS analysis of metals. CaCo-2 cell monolayers grown on Transwell inserts were washed twice with PBS, after which membranes were excised with a scalpel, transferred to 1.5 mL reaction tubes and frozen in liquid nitrogen. Cells were lysed by repeated freeze-thaw in 1 mL MilliQ-water and an aliquot of 25 µL was used to determine the cellular protein content according to the Lowry method (51) using BSA as a standard. An aliquot of 850 µL of the cell lysate was incubated with 300 µL HNO_3 (67-70%; BDH ARISTAR PLUS, VWR) at 85°C overnight followed by 2 h at 95°C and diluted to 7 mL with MilliQ-water. For the determination of the metal content in media, 10 mL of media were digested with 450 µL HNO_3. The digested samples and mice tissues were sent for ICP-MS analysis to the Arizona Laboratory for Emerging Contaminants (ALEC, Tucson, AZ, USA).

Immunocytochemistry & Confocal microscopy. CaCo-2 cell monolayers grown on Transwell inserts were washed twice with 2.6 mL (basolateral compartment) and 1.5 mL (apical compartment) ice-cold $PBS^{Ca/Mg}$ (PBS supplemented with 0.5 mM $MgCl_2$ and 0.9 mM $CaCl_2$, pH 7.2) and subsequently fixed with methanol for 15 min at -20 °C. After adding acetone (prechilled to -20 °C) for 30 s, cells were washed thrice (5 min each) with $PBS^{Ca/Mg}$. The membranes were excised with a scalpel, transferred to fresh 6-well plates and blocked with 1% BSA in $PBS^{Ca/Mg}$ for 2 h at RT. If not stated otherwise, the cells were washed thrice with $PBS^{Ca/Mg}$ in 5 min intervals between the different steps of the following staining procedure. Incubation of the membranes with rabbit anti-ZO1 (1:100) and mouse anti-Na^+, K^+ ATPase (1:100) was carried out at 4 °C over night in humidified atmosphere followed by an incubation with Alexa Fluor 488-conjugated goat anti-rabbit (1:500) and Alexa Fluor 594-conjugated goat anti-mouse antibodies (1:500) in 1% BSA in $PBS^{Ca/Mg}$ for 1 h at RT. To visualize the nuclei, the cells were exposed to 4′,6-diamidino-2-phenylindole dihydrochloride (DAPI, 1 µg x mL^{-1} in PBS) for 5 min at RT. The membranes were mounted on glass slides with cells facing up in ProLong Diamond Antifade Mountant (Thermo Fisher Scientific). A coverslip was placed on top of the cells and sealed with nail polish. Images were captured by a Zeiss LSM880 Inverted Confocal Microscope with a 63x oil objective at the Marley Imaging Core of the University of Arizona (Tucson, AZ, USA).

Integrity of the monolayer. Monolayer integrity of CaCo-2 cells was determined by the LY rejection assay. The cells were washed twice with 2.6 mL (basolateral compartment) and 1.5 mL (apical compartment) $PBS^{Ca/Mg}$ after which the inserts were transfered to fresh 6-well plates. 2.6 mL prewarmed

(37°C) salt-based incubation buffer (145 mM NaCl, 5.4 mM KCl, 1.8 mM $CaCl_2$, 1 mM $MgCl_2$, 0.8 mM Na_2HPO_4, 50 mM glucose, 20 mM PIPES) adjusted to pH 7.4 and 1.5 mL of prewarmed (37°C) incubation buffer containing 12.5 mg x mL^{-1} LY (Sigma-Aldrich) adjusted to pH 6.1 were added to the basolateral and apical compartment, respectively, and the cells were incubated for 4 h at 37°C in an incubator. An aliquot of 1 mL of incubation buffer was removed from the basolateral compartment every 60 minutes and replaced by the same volume of fresh incubation buffer adjusted to pH 7.4. At the end of the experiment the media from both compartments were collected. Standards containing 12.5 µg x mL^{-1} to 6.1 ng x mL^{-1} were prepared in incubation buffer adjusted to pH 7.4. Aliquots of 150 µL standard or sample were transferred into a well of a black microtiter plate and fluorescence was quantified using a BioTek Synergy 2 plate reader (BioTek Instruments Inc, Winooski, VT, USA). The pH of the media at the start and the end of the experiment was measured with a Sartorius pHCore pH meter (Sartorius, Lab Instruments GmbH & Co. KG, Goettingen, Germany).

Cell surface biotinylation. Cell surface biotinylation was performed on CaCo-2 cell monolayers grown on Transwell inserts. The cells were washed twice with 2.6 mL (basolateral compartment) and 1.5 mL (apical compartment) $PBS^{Ca/Mg}$ prewarmed to 37°C and twice with $PBS^{Ca/Mg}$ prechilled to 4°C after which the insert was transferred to a fresh 6-well plate. For biotinylation of basolateral (apical) surface proteins, 1.5 mL (1 mL) of freshly prepared, ice-cold solution containing 1 mg x mL^{-1} Sulfo-NHS-SS-biotin (Thermo Fisher Scientific) in $PBS^{Ca/Mg}$ was added to the basolateral (apical) compartment and 1 mL (1.5 mL) of ice-cold $PBS^{Ca/Mg}$ was added to the apical (basolateral) compartment. The cells were incubated on ice in an incubator at 4°C for 30 minutes with gentle rocking. The cells were then washed twice with 2.6 mL (basolateral compartment) and 1.5 mL (apical compartment) $PBS^{Ca/Mg}$ prechilled to 4°C. The reaction was quenched by incubating the cells with 2.6 mL (basolateral compartment) and 1.5 mL (apical compartment) 100 mM glycine in $PBS^{Ca/Mg}$ for 20 minutes on ice in an incubator at 4°C with gentle rocking. Again the cells were washed twice with 2.6 mL (basolateral compartment) and 1.5 mL (apical compartment) $PBS^{Ca/Mg}$ prechilled to 4°C. The insert was transferred to a fresh 6-well plate and the membrane was excised with a scalpel. The cells were lysed in 1 mL NETT buffer and the lysate was transferred into 1.5-mL reaction tubes. The lysate was chilled on ice for 20 minutes with vortexing every five minutes, sonicated with 10 strikes (2 s, amplitude 20) of a Q55 sonicator (Qsonica L.L.C, Newton, CT, USA) and centrifuged (15000 x g, 4°C, 15 min). The supernatant was transferred into fresh 1.5 mL reaction tubes. An aliquot of 150 µL (total protein) was frozen in liquid nitrogen and stored at -80°C for later immunoblot analysis and 850 µL of the lysates were transferred to Pierce™ centrifuge columns that had been preloaded with 100 µL of Pierce™ High Capacity NeutrAvidin™ Agarose (both from Thermo Fisher Scientific) according to the manufactures protocol. The samples were incubated overnight at 4°C with slight rocking motion after which the supernatant was removed by centrifugation for 1 minute at RT and 1500 x g. The agarose beads were washed once with NETT containing protease inhibitor, two times with NETT buffer without protease inhibitor, two times with salt wash buffer (350 mM NaCl, 5 mM EDTA, 0.1% Triton X-100 in PBS, pH 7.4) and three times with NET buffer (150 mM NaCl, 5 mM EDTA, 10 mM Tris, pH 7.4). Between the individual washing steps the supernatant was removed by centrifugation for 1 minute at RT and 1500 x g. To elute the biotinylated proteins 100 µL of 1x Sample buffer [1.7 % (w/v) SDS, 5% (v/v) glycerol, 150 mM DTT, 58 mM Tris, pH 6.8] was added to the agarose beads and the samples were incubated at 4°C overnight. On the next day the centifuge columns were placed in fresh 1.5 mL reaction tubes, incubated for 30 minutes at 37°C and centrifuged for 2 minutes at RT and 1500 x g. The eluate (surface protein) was transferred to fresh 1.5 mL reaction tubes, frozen in liquid nitrogen and stored at -80°C for later immunoblot analysis.

Preparation of radiolabeled metal solutions. Radiolabeled metal solutions were prepared on the day of the experiment. Five-times concentrated (0.5 µM) radiolabeled Mn solutions were prepared from $^{54}MnCl_2$ (PerkinElmer Inc., Waltham, MA, USA) complexed to citrate prior to addition to DMEM. Five-times concentrated (5 µM) radiolabeled Fe(II) solutions were prepared from $^{59}FeCl_3$ (PerkinElmer Inc.) that had been reduced by 5 mM ascorbate prior

to addition to DMEM containing 5 mM ascorbate. Five-times concentrated (5 μM) radiolabeled Fe(III) solutions were prepared from $^{59}FeCl_3$ that had been complexed to citrate prior to addition to DMEM.

Metal uptake and transport. Metal uptake and transport was studied in CaCo-2 cell monolayers grown on Transwell inserts. During the experiments cells were incubated at 37°C in the humified atmosphere of an incubator and all solutions required before the termination of the experiment were prewarmed to 37°C. At the start of the experiments cells were washed twice with 2.6 mL (basolateral compartment) and 1.5 mL (apical compartment) $PBS^{Ca/Mg}$. The inserts were then transferred to fresh 6-well plates. If not stated otherwise, 2.6 mL transport medium (DMEM containing 1 mM pyruvate supplemented with 20 mM PIPES) adjusted to pH 7.4 and 1.5 mL tranport medium adjusted to pH 6.1 were added to the basolateral and apical compartment, respectively, and the cells were preincubated for 30 minutes. Basolateral (apical) metal uptake and basolateral-to-apical (apical-to-basolateral) transport experiments were initiated by replacing 520 μL (300 μL) transport medium of the basolateral (apical) compartment by the same volume of a freshly prepared five-times concentrated radiolabeled metal solution and the cells were incubated for the desired times. When basolateral-to-apical (apical-to-basolateral) transport was studied an aliquot of 1 mL of medium was removed from the apical (basolateral) compartment for γ-counting by a 2480 WIZARD^2 Automatic Gamma Counter (PerkinElmer Inc.) and replaced by the same volume of the media initially added to the compartment at the time points indicated in the figures. The experiments were stopped by aspirating the media from both compartments and washing the cells three times with ice-cold PBS supplemented with 1 mM EDTA. The cells were lysed in 1 mL 0.5 M NaOH and an aliquot of 25 μL was used to determine the cellular protein content according to the Lowry method (51) using BSA as a standard. An aliquot of 200 μL to 800 μL of the lysate were used to quantify the cellular contents of ^{54}Mn and ^{59}Fe by γ-counting.

Statistical analysis. Significance of differences between two sets of data were analyzed using Student's *t*-test. Comparisons between multiple sets of data were performed using one- or two-way analysis of variance (ANOVA) followed by the Bonferroni post-hoc test, with $*p < 0.05$, $**p < 0.01$ and $***p < 0.001$. $p > 0.05$ was considered as not significant. The PRISM 5 software (GraphPad, La Jolla, CA, USA) was used for statistical analysis.

Acknowledgments: This work was supported by the National Institutes of Health Grants R00DK104066 (to N.Z.). We thank Dr. Dennis Bernd Nestvogel and Dani Felber for critical reading of the manuscript. We thank Mary Kay Amistadi in the Arizona Laboratory for Emerging Contaminants with the help of ICP-MS measurement. We thank Patty Jansma in the Marley Imaging Core of the University of Arizona for helping us with the acquisition of confocal images.

Conflict of interest: The authors declare that they have no conflicts of interest with the contents of this article.

The content is solely the responsibility of the authors and does not necessarily represent the official views of the National Institutes of Health.

References

1. Avila, D. S., Puntel, R. L., and Aschner, M. (2013) Manganese in health and disease. Met Ions Life Sci 13, 199-227
2. Wedler, F. C. (1994) Biochemical and nutritional role of manganese: an overview. FL, 1-37
3. Weigand, E., Kirchgessner, M., and Helbig, U. (1986) True absorption and endogenous fecal excretion of manganese in relation to its dietary supply in growing rats. Biol Trace Elem Res 10, 265-279
4. Britton, A. A., and Cotzias, G. C. (1966) Dependence of manganese turnover on intake. Am J Physiol 211, 203-206
5. Dorman, D. C., Struve, M. F., James, R. A., McManus, B. E., Marshall, M. W., and Wong, B. A. (2001) Influence of dietary manganese on the pharmacokinetics of inhaled manganese sulfate in male CD rats. Toxicol Sci 60, 242-251
6. Davis, C. D., Wolf, T. L., and Greger, J. L. (1992) Varying levels of manganese and iron affect absorption and gut endogenous losses of manganese by rats. J Nutr 122, 1300-1308
7. Finley, J. W., Johnson, P. E., and Johnson, L. K. (1994) Sex affects manganese absorption and retention by humans from a diet adequate in manganese. Am J Clin Nutr 60, 949-955
8. Teeguarden, J. G., Dorman, D. C., Covington, T. R., Clewell, H. J., 3rd, and Andersen, M. E. (2007) Pharmacokinetic modeling of manganese. I. Dose dependencies of uptake and elimination. J Toxicol Environ Health A 70, 1493-1504
9. Horning, K. J., Caito, S. W., Tipps, K. G., Bowman, A. B., and Aschner, M. (2015) Manganese Is Essential for Neuronal Health. Annu Rev Nutr 35, 71-108
10. Tuschl, K., Meyer, E., Valdivia, L. E., Zhao, N., Dadswell, C., Abdul-Sada, A., Hung, C. Y., Simpson, M. A., Chong, W. K., Jacques, T. S., Woltjer, R. L., Eaton, S., Gregory, A., Sanford, L., Kara, E., Houlden, H., Cuno, S. M., Prokisch, H., Valletta, L., Tiranti, V., Younis, R., Maher, E. R., Spencer, J., Straatman-Iwanowska, A., Gissen, P., Selim, L. A., Pintos-Morell, G., Coroleu-Lletget, W., Mohammad, S. S., Yoganathan, S., Dale, R. C., Thomas, M., Rihel, J., Bodamer, O. A., Enns, C. A., Hayflick, S. J., Clayton, P. T., Mills, P. B., Kurian, M. A., and Wilson, S. W. (2016) Mutations in SLC39A14 disrupt manganese homeostasis and cause childhood-onset parkinsonism-dystonia. Nat Commun 7, 11601
11. Boycott, K. M., Beaulieu, C. L., Kernohan, K. D., Gebril, O. H., Mhanni, A., Chudley, A. E., Redl, D., Qin, W., Hampson, S., Kury, S., Tetreault, M., Puffenberger, E. G., Scott, J. N., Bezieau, S., Reis, A., Uebe, S., Schumacher, J., Hegele, R. A., McLeod, D. R., Galvez-Peralta, M., Majewski, J., Ramaekers, V. T., Nebert, D. W., Innes, A. M., Parboosingh, J. S., Abou Jamra, R., and Consortium, C. R. C. (2015) Autosomal-Recessive Intellectual Disability with Cerebellar Atrophy Syndrome Caused by Mutation of the Manganese and Zinc Transporter Gene SLC39A8. Am J Hum Genet 97, 886-893
12. Park, J. H., Hogrebe, M., Gruneberg, M., DuChesne, I., von der Heiden, A. L., Reunert, J., Schlingmann, K. P., Boycott, K. M., Beaulieu, C. L., Mhanni, A. A., Innes, A. M., Hurtnagel, K., Biskup, S., Gleixner, E. M., Kurlemann, G., Fiedler, B., Omran, H., Rutsch, F., Wada, Y., Tsiakas, K., Santer, R., Nebert, D. W., Rust, S., and Marquardt, T. (2015) SLC39A8 Deficiency: A Disorder of Manganese Transport and Glycosylation. Am J Hum Genet 97, 894-903
13. Quadri, M., Federico, A., Zhao, T., Breedveld, G. J., Battisti, C., Delnooz, C., Severijnen, L. A., Mammarella, L. D. T., Mignarri, A., Monti, L., Sanna, A., Lu, P., Punzo, F., Cossu, G., Willemsen, R., Rasi, F., Oostra, B. A., van de Warrenburg, B. P., and Bonifati, V. (2012) Mutations in SLC30A10 Cause Parkinsonism and Dystonia with Hypermanganesemia, Polycythemia, and Chronic Liver Disease. Am J Hum Genet 90, 467-477
14. Tuschl, K., Clayton, P. T., Gospe, S. M., Gulab, S., Ibrahim, S., Singhi, P., Aulakh, R., Ribeiro, R. T., Barsottini, O. G., Zaki, M. S., Del Rosario, M. L., Dyack, S., Price, V., Rideout, A., Gordon, K., Wevers, R. A., Chong, W. K., and Mills, P. B. (2012) Syndrome of Hepatic Cirrhosis, Dystonia, Polycythemia, and Hypermanganesemia Caused by Mutations in SLC30A10, a Manganese Transporter in Man. Am J Hum Genet 90, 457-466

15. Girijashanker, K., He, L., Soleimani, M., Reed, J. M., Li, H., Liu, Z., Wang, B., Dalton, T. P., and Nebert, D. W. (2008) Slc39a14 gene encodes ZIP14, a metal/bicarbonate symporter: similarities to the ZIP8 transporter. Mol Pharmacol 73, 1413-1423
16. Rodan, L. H., Hauptman, M., D'Gama, A. M., Qualls, A. E., Cao, S., Tuschl, K., Al-Jasmi, F., Hertecant, J., Hayflick, S. J., Wessling-Resnick, M., Yang, E. T., Berry, G. T., Gropman, A., Woolf, A. D., and Agrawal, P. B. (2018) Novel founder intronic variant in SLC39A14 in two families causing Manganism and potential treatment strategies. Mol Genet Metab 124, 161-167
17. Marti-Sanchez, L., Ortigoza-Escobar, J. D., Darling, A., Villaronga, M., Baide, H., Molero-Luis, M., Batllori, M., Vanegas, M. I., Muchart, J., Aquino, L., Artuch, R., Macaya, A., Kurian, M. A., and Duenas, P. (2018) Hypermanganesemia due to mutations in SLC39A14: further insights into Mn deposition in the central nervous system. Orphanet J Rare Dis 13, 28
18. Juneja, M., Shamim, U., Joshi, A., Mathur, A., Uppili, B., Sairam, S., Ambawat, S., Dixit, R., and Faruq, M. (2018) A novel mutation in SLC39A14 causing hypermanganesemia associated with infantile onset dystonia. J Gene Med 20, e3012
19. Xin, Y., Gao, H., Wang, J., Qiang, Y., Imam, M. U., Li, Y., Wang, J., Zhang, R., Zhang, H., Yu, Y., Wang, H., Luo, H., Shi, C., Xu, Y., Hojyo, S., Fukada, T., Min, J., and Wang, F. (2017) Manganese transporter Slc39a14 deficiency revealed its key role in maintaining manganese homeostasis in mice. Cell Discov 3, 17025
20. Liu, C., Hutchens, S., Jursa, T., Shawlot, W., Polishchuk, E. V., Polishchuk, R. S., Dray, B. K., Gore, A. C., Aschner, M., Smith, D. R., and Mukhopadhyay, S. (2017) Hypothyroidism induced by loss of the manganese efflux transporter SLC30A10 may be explained by reduced thyroxine production. J Biol Chem 292, 16605-16615
21. Aydemir, T. B., Kim, M. H., Kim, J., Colon-Perez, L. M., Banan, G., Mareci, T. H., Febo, M., and Cousins, R. J. (2017) Metal Transporter Zip14 (Slc39a14) Deletion in Mice Increases Manganese Deposition and Produces Neurotoxic Signatures and Diminished Motor Activity. J Neurosci 37, 5996-6006
22. Jenkitkasemwong, S., Akinyode, A., Paulus, E., Weiskirchen, R., Hojyo, S., Fukada, T., Giraldo, G., Schrier, J., Garcia, A., Janus, C., Giasson, B., and Knutson, M. D. (2018) SLC39A14 deficiency alters manganese homeostasis and excretion resulting in brain manganese accumulation and motor deficits in mice. Proc Natl Acad Sci U S A 115, E1769-E1778
23. Liuzzi, J. P., Aydemir, F., Nam, H., Knutson, M. D., and Cousins, R. J. (2006) Zip14 (Slc39a14) mediates non-transferrin-bound iron uptake into cells. Proc Natl Acad Sci U S A 103, 13612-13617
24. Uhlen, M., Fagerberg, L., Hallstrom, B. M., Lindskog, C., Oksvold, P., Mardinoglu, A., Sivertsson, A., Kampf, C., Sjostedt, E., Asplund, A., Olsson, I., Edlund, K., Lundberg, E., Navani, S., Szigyarto, C. A., Odeberg, J., Djureinovic, D., Takanen, J. O., Hober, S., Alm, T., Edqvist, P. H., Berling, H., Tegel, H., Mulder, J., Rockberg, J., Nilsson, P., Schwenk, J. M., Hamsten, M., von Feilitzen, K., Forsberg, M., Persson, L., Johansson, F., Zwahlen, M., von Heijne, G., Nielsen, J., and Ponten, F. (2015) Proteomics. Tissue-based map of the human proteome. Science 347, 1260419
25. Hubatsch, I., Ragnarsson, E. G., and Artursson, P. (2007) Determination of drug permeability and prediction of drug absorption in Caco-2 monolayers. Nat Protoc 2, 2111-2119
26. Sandberg, A. S. (2010) The use of caco-2 cells to estimate fe absorption in humans--a critical appraisal. Int J Vitam Nutr Res 80, 307-313
27. Bentz, J., O'Connor, M. P., Bednarczyk, D., Coleman, J., Lee, C., Palm, J., Pak, Y. A., Perloff, E. S., Reyner, E., Balimane, P., Brannstrom, M., Chu, X. Y., Funk, C., Guo, A. L., Hanna, I., Heredi-Szabo, K., Hillgren, K., Li, L. B., Hollnack-Pusch, E., Jamei, M., Lin, X. N., Mason, A. K., Neuhoff, S., Patel, A., Podila, L., Plise, E., Rajaraman, G., Salphati, L., Sands, E., Taub, M. E., Taur, J. S., Weitz, D., Wortelboer, H. M., Xia, C. Q., Xiao, G. Q., Yabut, J., Yamagata, T., Zhang, L., and Ellens, H. (2013) Variability in P-Glycoprotein Inhibitory Potency (IC50) Using Various in Vitro Experimental Systems: Implications for Universal Digoxin Drug-Drug Interaction Risk Assessment Decision Criteria. Drug Metabolism and Disposition 41, 1347-1366

28. Gunshin, H., Mackenzie, B., Berger, U. V., Gunshin, Y., Romero, M. F., Boron, W. F., Nussberger, S., Gollan, J. L., and Hediger, M. A. (1997) Cloning and characterization of a mammalian proton-coupled metal-ion transporter. Nature 388, 482-488
29. Tandy, S., Williams, M., Leggett, A., Lopez-Jimenez, M., Dedes, M., Ramesh, B., Srai, S. K., and Sharp, P. (2000) Nramp2 expression is associated with pH-dependent iron uptake across the apical membrane of human intestinal Caco-2 cells. J Biol Chem 275, 1023-1029
30. Hoch, E., and Sekler, I. (2018) Elucidating the H+ coupled Zn2+ transport mechanism of ZIP4; implications in Acrodermatitis Enteropathica,
31. Guthrie, G. J., Aydemir, T. B., Troche, C., Martin, A. B., Chang, S. M., and Cousins, R. J. (2015) Influence of ZIP14 (slc39A14) on intestinal zinc processing and barrier function. Am J Physiol Gastrointest Liver Physiol 308, G171-178
32. Rahelic, D., Kujundzic, M., Romic, Z., Brkic, K., and Petrovecki, M. (2006) Serum concentration of zinc, copper, manganese and magnesium in patients with liver cirrhosis. Coll Antropol 30, 523-528
33. Pinilla-Tenas, J. J., Sparkman, B. K., Shawki, A., Illing, A. C., Mitchell, C. J., Zhao, N., Liuzzi, J. P., Cousins, R. J., Knutson, M. D., and Mackenzie, B. (2011) Zip14 is a complex broad-scope metal-ion transporter whose functional properties support roles in the cellular uptake of zinc and nontransferrin-bound iron. Am J Physiol Cell Physiol 301, C862-871
34. Zhao, N., Gao, J., Enns, C. A., and Knutson, M. D. (2010) ZRT/IRT-like protein 14 (ZIP14) promotes the cellular assimilation of iron from transferrin. J Biol Chem 285, 32141-32150
35. Canonne-Hergaux, F., Gruenheid, S., Ponka, P., and Gros, P. (1999) Cellular and subcellular localization of the Nramp2 iron transporter in the intestinal brush border and regulation by dietary iron. Blood 93, 4406-4417
36. Shawki, A., Anthony, S. R., Nose, Y., Engevik, M. A., Niespodzany, E. J., Barrientos, T., Ohrvik, H., Worrell, R. T., Thiele, D. J., and Mackenzie, B. (2015) Intestinal DMT1 is critical for iron absorption in the mouse but is not required for the absorption of copper or manganese. Am J Physiol Gastrointest Liver Physiol 309, G635-647
37. Knopfel, M., Zhao, L., and Garrick, M. D. (2005) Transport of divalent transition-metal ions is lost in small-intestinal tissue of b/b Belgrade rats. Biochemistry 44, 3454-3465
38. Chua, A. C., and Morgan, E. H. (1997) Manganese metabolism is impaired in the Belgrade laboratory rat. J Comp Physiol B 167, 361-369
39. Geszvain, K., Butterfield, C., Davis, R. E., Madison, A. S., Lee, S. W., Parker, D. L., Soldatova, A., Spiro, T. G., Luther, G. W., and Tebo, B. M. (2012) The molecular biogeochemistry of manganese(II) oxidation. Biochem Soc Trans 40, 1244-1248
40. Missy, P., Lanhers, M. C., Grignon, Y., Joyeux, M., and Burnel, D. (2000) In vitro and in vivo studies on chelation of manganese. Hum Exp Toxicol 19, 448-456
41. Jayasena, T., Grant, R. S., Keerthisinghe, N., Solaja, I., and Smythe, G. A. (2007) Membrane permeability of redox active metal chelators: an important element in reducing hydroxyl radical induced NAD+ depletion in neuronal cells. Neurosci Res 57, 454-461
42. Bannon, D. I., Abounader, R., Lees, P. S., and Bressler, J. P. (2003) Effect of DMT1 knockdown on iron, cadmium, and lead uptake in Caco-2 cells. Am J Physiol Cell Physiol 284, C44-50
43. Hennigar, S. R., and McClung, J. P. (2016) Hepcidin Attenuates Zinc Efflux in Caco-2 Cells. J Nutr 146, 2167-2173
44. Li, X., Xie, J., Lu, L., Zhang, L., Zhang, L., Zou, Y., Wang, Q., Luo, X., and Li, S. (2013) Kinetics of manganese transport and gene expressions of manganese transport carriers in Caco-2 cell monolayers. Biometals 26, 941-953
45. Leblondel, G., and Allain, P. (1999) Manganese transport by Caco-2 cells. Biol Trace Elem Res 67, 13-28
46. Finley, J. W., and Monroe, P. (1997) Mn absorption: The use of CACO-2 cells as a model of the intestinal epithelia. J Nutr Biochem 8, 92-101

47. Klein, L. D., Breakey, A. A., Scelza, B., Valeggia, C., Jasienska, G., and Hinde, K. (2017) Concentrations of trace elements in human milk: Comparisons among women in Argentina, Namibia, Poland, and the United States. PLoS One 12, e0183367
48. Lonnerdal, B., Keen, C. L., Ohtake, M., and Tamura, T. (1983) Iron, zinc, copper, and manganese in infant formulas. Am J Dis Child 137, 433-437
49. Ran, F. A., Hsu, P. D., Wright, J., Agarwala, V., Scott, D. A., and Zhang, F. (2013) Genome engineering using the CRISPR-Cas9 system. Nat Protoc 8, 2281-2308
50. Cong, L., Ran, F. A., Cox, D., Lin, S., Barretto, R., Habib, N., Hsu, P. D., Wu, X., Jiang, W., Marraffini, L. A., and Zhang, F. (2013) Multiplex genome engineering using CRISPR/Cas systems. Science 339, 819-823
51. Lowry, O. H., Rosebrough, N. J., Farr, A. L., and Randall, R. J. (1951) Protein measurement with the Folin phenol reagent. J Biol Chem 193, 265-275
52. Taylor, C. A., Hutchens, S., Liu, C., Jursa, T., Shawlot, W., Aschner, M., Smith, D. R., and Mukhopadhyay, S. (2019) SLC30A10 transporter in the digestive system regulates brain manganese under basal conditions while brain SLC30A10 protects against neurotoxicity. J. Biol. Chem. 294, 1860–1876

FOOTNOTES

The abbreviations used are: ANOVA, analysis of variance; BSA, bovine serum albumin; CRISPR, clustered regularly interspaced short palindromic repeats; DAPI, 4′,6-diamidino-2-phenylindole; DFO, desferrioxamine; DMEM, Dulbecco's Modified Eagle Medium; DMT1, divalent metal transporter 1; EDTA, ethylenediaminetetraacetic acid; FITC, fluorescein isothiocyanate; GAPDH, glyceraldehyde 3-phosphate dehydrogenase; gRNA, guide RNA; GST, glutathione S-transferase; HRP, horseradish peroxidase; ICP-MS, inductively coupled plasma mass spectrometry; IgG, immunoglobulin G; KO, knock-out; LY, Lucifer yellow; P_{app}, apparent permeability; PBS, phosphate-buffered saline; PIPES, piperazine-N,N′-bis(2-ethanesulfonic acid); RNAi, RNA interference; RT, room temperature; SLC, solute carrier; TBS, tris-buffered saline; WT, wild type; ZIP, Zrt- and Irt-like protein; ZnT, Zn transporter; ZO-1, Zonula occludens-1.

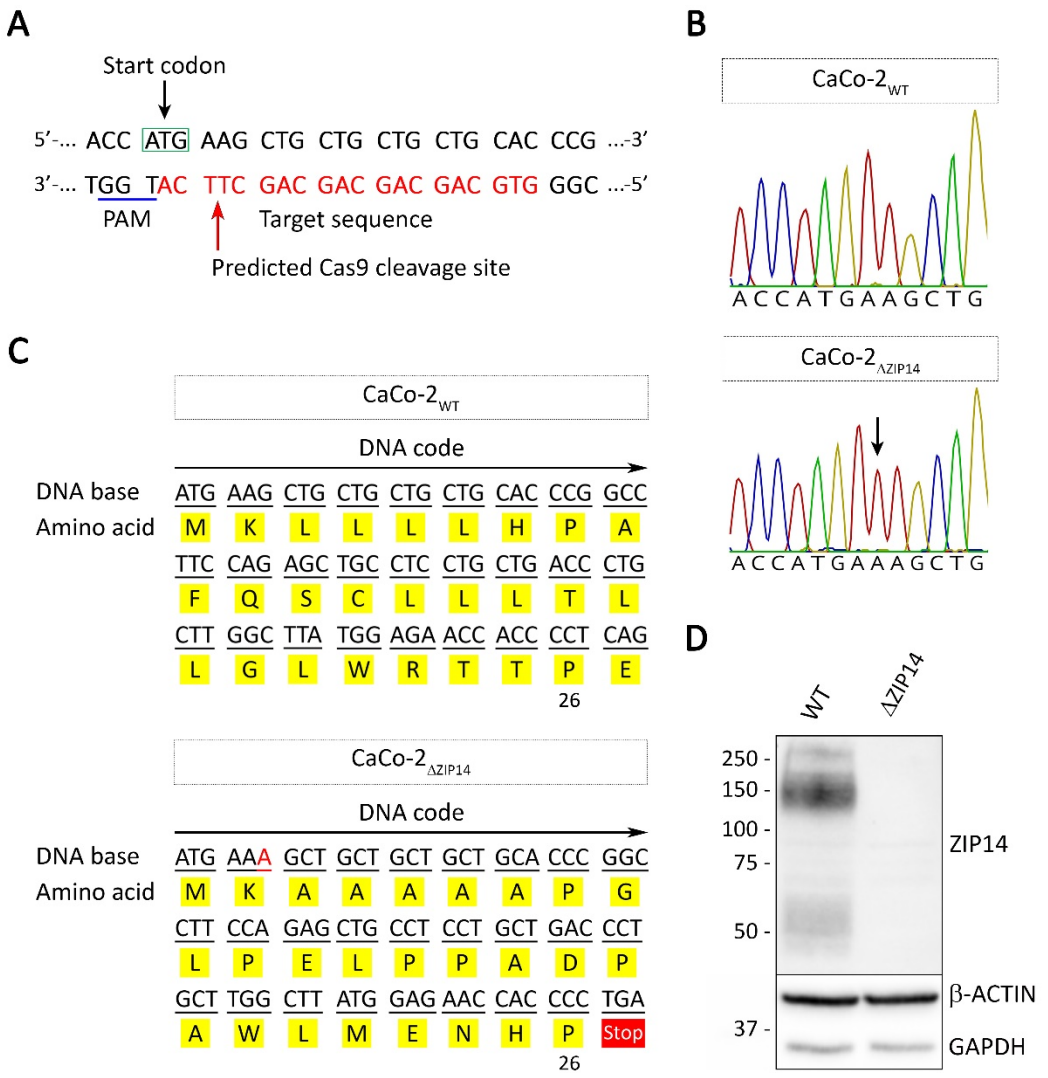

Figure 1. Generation of a *ZIP14* KO CaCo-2 cell line (CaCo-$2_{\Delta ZIP14}$). (A) Schematic illustration of CRISPR/Cas9-mediated genome editing to generate CaCo-$2_{\Delta ZIP14}$ cells. The DNA sequence covering the start codon of *ZIP14* within exon 2 is shown. The guide RNA (gRNA) sequence is marked in red letters and the PAM (protospacer adjacent motif) sequence is underlined in blue. The red arrow marks the predicted Cas9 cleavage site. (B) Chromatograms of sequencing results using DNA isolated from CaCo-2_{WT} and CaCo-$2_{\Delta ZIP14}$ cells. The black arrow indicates the insertion of an adenosine at the predicted Cas9 cleavage site. (C) The single adenosine-insertion results in a frameshift with premature translation termination after amino acid 26. (D) ZIP14 immunoblot of whole-cell lysates of CaCo-2_{WT} (WT) and CaCo-$2_{\Delta ZIP14}$ (ΔZIP14) cells confirms the deletion of ZIP14 in CaCo-$2_{\Delta ZIP14}$ cells. Both β-ACTIN and GAPDH were used as loading controls.

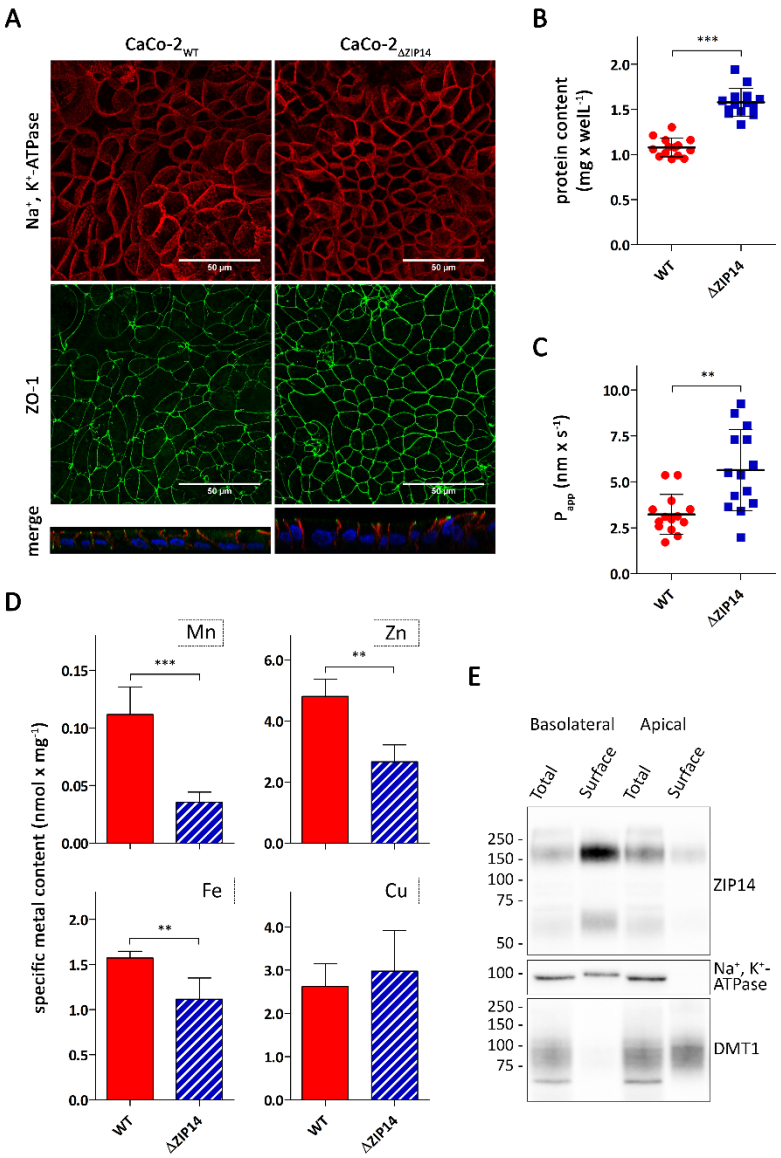

Figure 2. Characterization of CaCo-2_{WT} and CaCo-$2_{\Delta ZIP14}$ transwell cultures. (A) Confocal microscopy of CaCo-2_{WT} and CaCo-$2_{\Delta ZIP14}$ cells co-immunostained for Na^+, K^+-ATPase and ZO-1. Nuclei were stained with DAPI. The four upper panels show the orthogonal maximum projections of 42- and 69-frames stacks for CaCo-2_{WT} and CaCo-$2_{\Delta ZIP14}$ cells, respectively. The two bottom panels show a perpendicular projection of merged Na^+, K^+-ATPase (red) and ZO-1 (green) proteins with nuclei (blue). The scale bars (50 µm) in the upper panels also apply to the bottom panels (B) Total protein content, (C) apparent permeability (P_{app}) of Lucifer Yellow and (D) specific contents of Mn, Zn, Fe and Cu of CaCo-2_{WT} (WT) and CaCo-$2_{\Delta ZIP14}$ (ΔZIP14) transwell cultures. Data are presented as means ± s.d. from (B, C) 13 or (D) 3 independent prepared cultures. Statistical analysis was performed using Student's *t*-test with $^{**}p < 0.01$ and $^{***}p < 0.001$. (E) CaCo-2_{WT} transwell cultures were subjected to basolateral or apical surface biotinylation with cell membrane impermeable Sulfo-NHS-SS-biotin. Biotin-labeled cell-surface proteins (Surface) were isolated from whole-cell lysates (Total) using NeutrAvidin agarose beads. 45 µg whole-cell lysates (Total) and 15 µg Biotin-labeled cell-surface proteins (Surface) were analyzed by immunoblotting for ZIP14. Na^+, K^+-ATPase served as the basolateral marker and DMT1 as the apical marker.

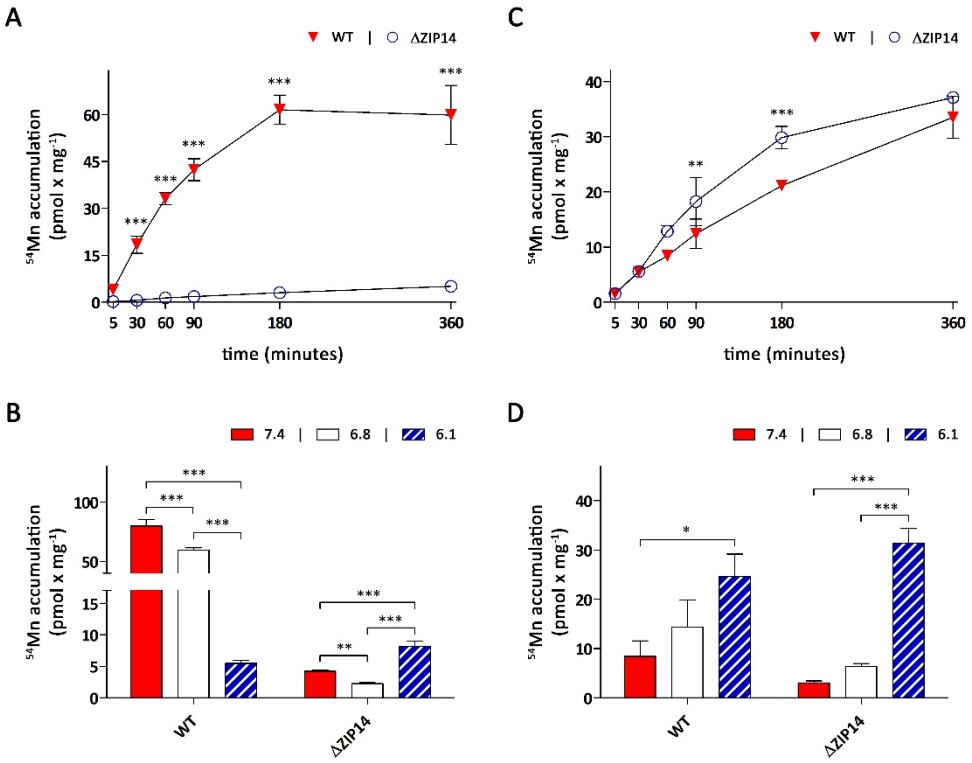

Figure 3. Mn uptake by CaCo-2_{WT} and CaCo-$2_{\Delta ZIP14}$ monolayers. Uptake experiments were initiated by adding Mn-citrate spiked with ^{54}Mn either to the (A, B) basolateral or (C, D) apical compartment. (A, C). Time-dependence of Mn uptake by CaCo-2_{WT} (WT) and CaCo-$2_{\Delta ZIP14}$ (ΔZIP14) cells in the presence of 0.1 µM ^{54}Mn-citrate. During the uptake experiments the extracellular pH was maintained at pH 7.4 in the basolateral and pH 6.1 in the apical compartment. (B, D) pH-dependence of Mn uptake by WT and ΔZIP14 cells. The cells were incubated for four hours in the presence of 0.1 µM ^{54}Mn-citrate. During the experiments the pH of both the apical and basolateral compartment was maintained at the pH indicated in the figures. Data are presented as means ± s.d. from three independent experiments performed in duplicates. Statistical analysis was performed using two-way ANOVA followed by the Bonferroni post-hoc test with *$p < 0.05$, **$p < 0.01$ and ***$p < 0.001$.

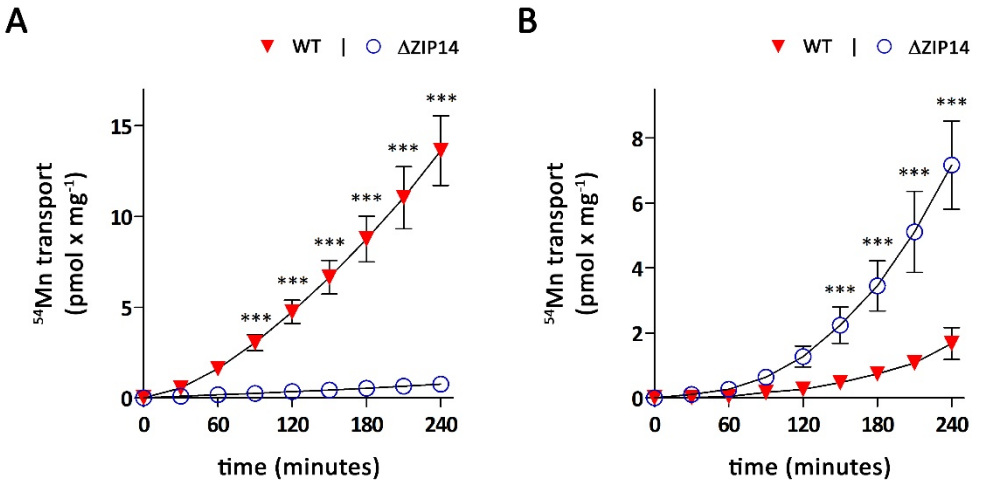

Figure 4. Mn transport by CaCo-2_{WT} and CaCo-$2_{\Delta ZIP14}$ monolayers. Mn-transport experiments were initiated by adding 0.1 µM ^{54}Mn-citrate either to the (A) basolateral or (B) apical compartment of CaCo-2_{WT} (WT) and CaCo-$2_{\Delta ZIP14}$ (ΔZIP14) monolayers. Samples were collected every 30 min from the opposite compartment and analyzed by γ-counting. During the transport experiments the extracellular pH was maintained at pH 7.4 in the basolateral and pH 6.1 in the apical compartment. Data are presented as means ± s.d. from three independent experiments performed in duplicates. Statistical analysis was performed using two-way ANOVA followed by the Bonferroni post-hoc test with ***$p < 0.001$.

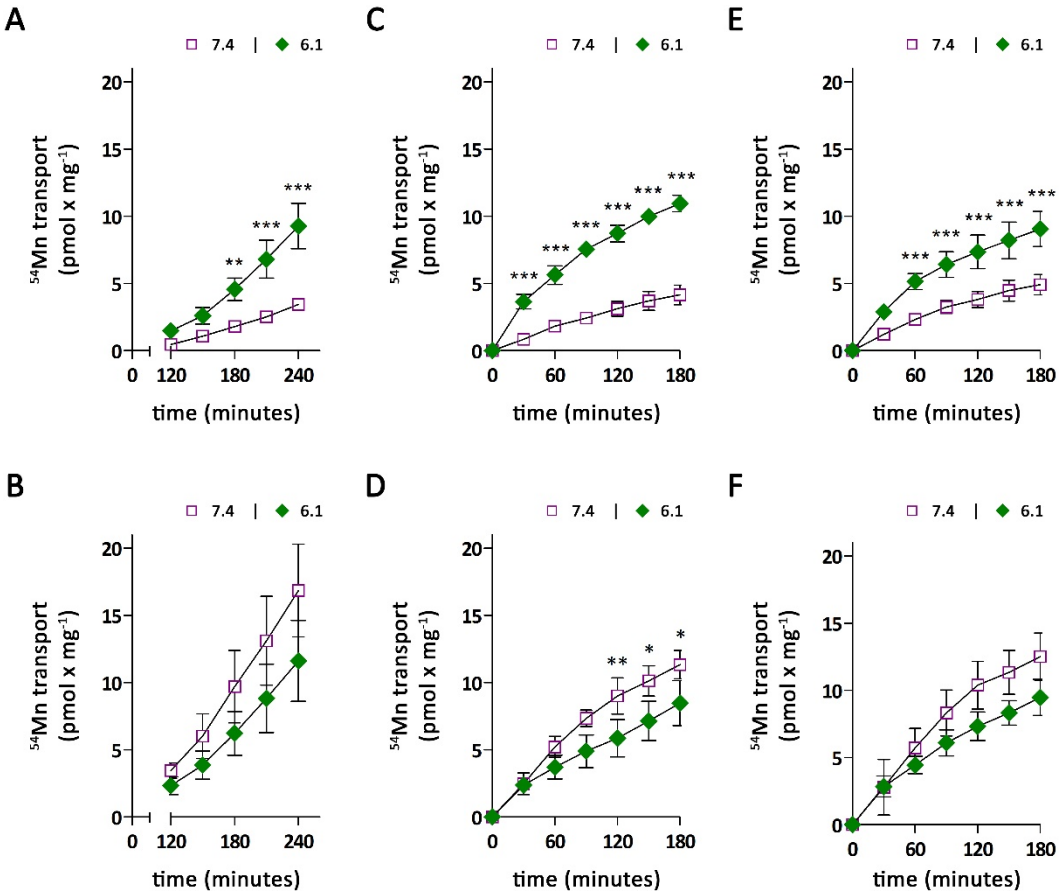

Figure 5. Modulation of apical to basolateral Mn transport by extracellular pH. Mn-transport experiments were initiated by adding 0.1 µM ^{54}Mn-citrate to the apical compartment of (A, C, E) CaCo-2_{WT} and (B, D, F) CaCo-$2_{\Delta ZIP14}$ monolayers. Throughout the transport experiments the extracellular pH in the apical compartment was maintained at pH 6.1. (A, B) The cells were incubated for 240 minutes maintaining the basolateral pH at either pH 7.4 or pH 6.1. Samples were collected between 120 and 240 minutes for γ-counting. (C - F) The cells were loaded for 240 minutes with 0.1 µM ^{54}Mn-citrate from the apical side with the basolateral pH maintained at (C, D) pH 7.4 or (E, F) pH 6.1. Subsequently ^{54}Mn was removed, the cells were washed thrice with PBS$^{Ca/Mg}$ from both sides and transferred to fresh 6-well plates. The accumulation of ^{54}Mn in the basolateral compartment was followed for another 180 minutes, with the pH of the basolateral compartment either maintained at pH 7.4 or at pH 6.1. Data are presented as means ± s.d. from three independent experiments. Statistical analysis was performed using two-way ANOVA followed by the Bonferroni post-hoc test with *$p < 0.05$, **$p < 0.01$ and ***$p < 0.001$.

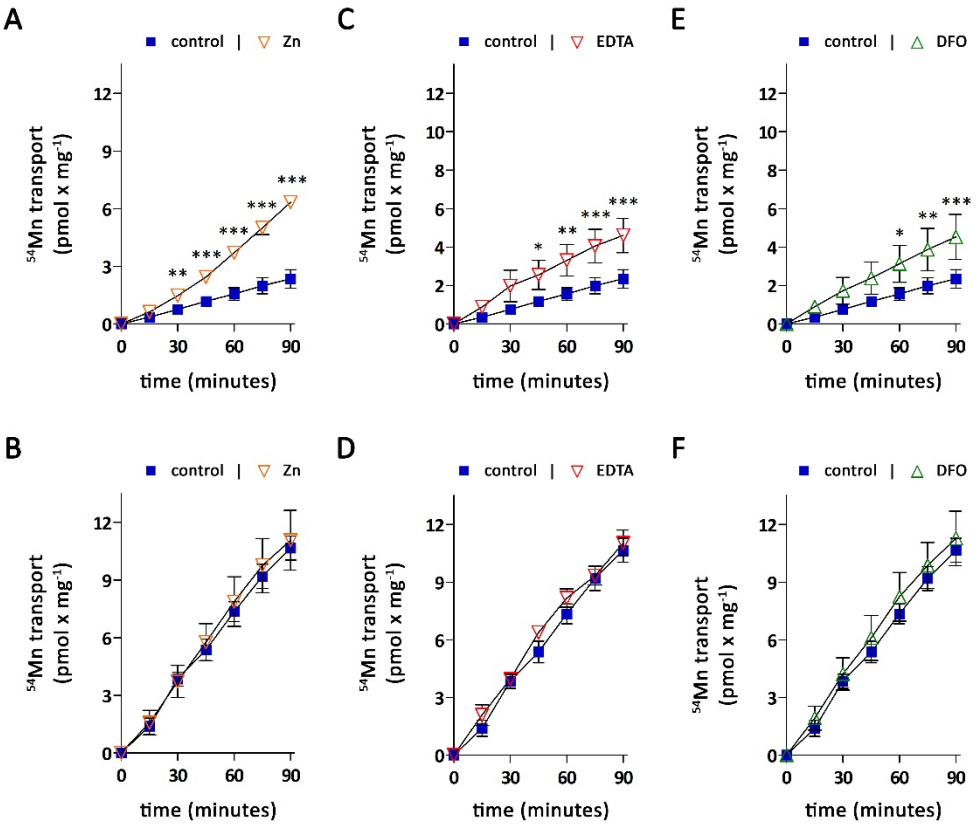

Figure 6. Modulation of apical to basolateral Mn transport by Zn competition or chelators. Mn-transport experiments were initiated by adding 0.1 µM ^{54}Mn-citrate to the apical compartment of (A, C, E) CaCo-2_{WT} and (B, D, F)) CaCo-$2_{\Delta ZIP14}$ monolayers. Throughout the transport experiments the extracellular pH in the apical compartment was maintained at pH 6.1. The cells were loaded for 240 minutes with 0.1 µM ^{54}Mn-citrate from the apical side with the basolateral pH maintained at pH 7.4. Subsequently ^{54}Mn was removed, the cells were washed thrice with PBS$^{Ca/Mg}$ from both sides and transferred to fresh 6-well plates. The basolateral medium was changed from DMEM to salt-based incubation buffer adjusted to pH 7.4 (control) containing (A, B) 2 µM $ZnCl_2$, (C, D) 100 µM $CaNa_2EDTA$ or (E, F) 1 mM desferrioxamine (DFO) and the accumulation of ^{54}Mn in the basolateral compartment was followed for another 90 minutes. Data are presented as means ± s.d. from three independent experiments. Statistical analysis was performed using two-way ANOVA followed by the Bonferroni post-hoc test with *$p < 0.05$, **$p < 0.01$ and ***$p < 0.001$.

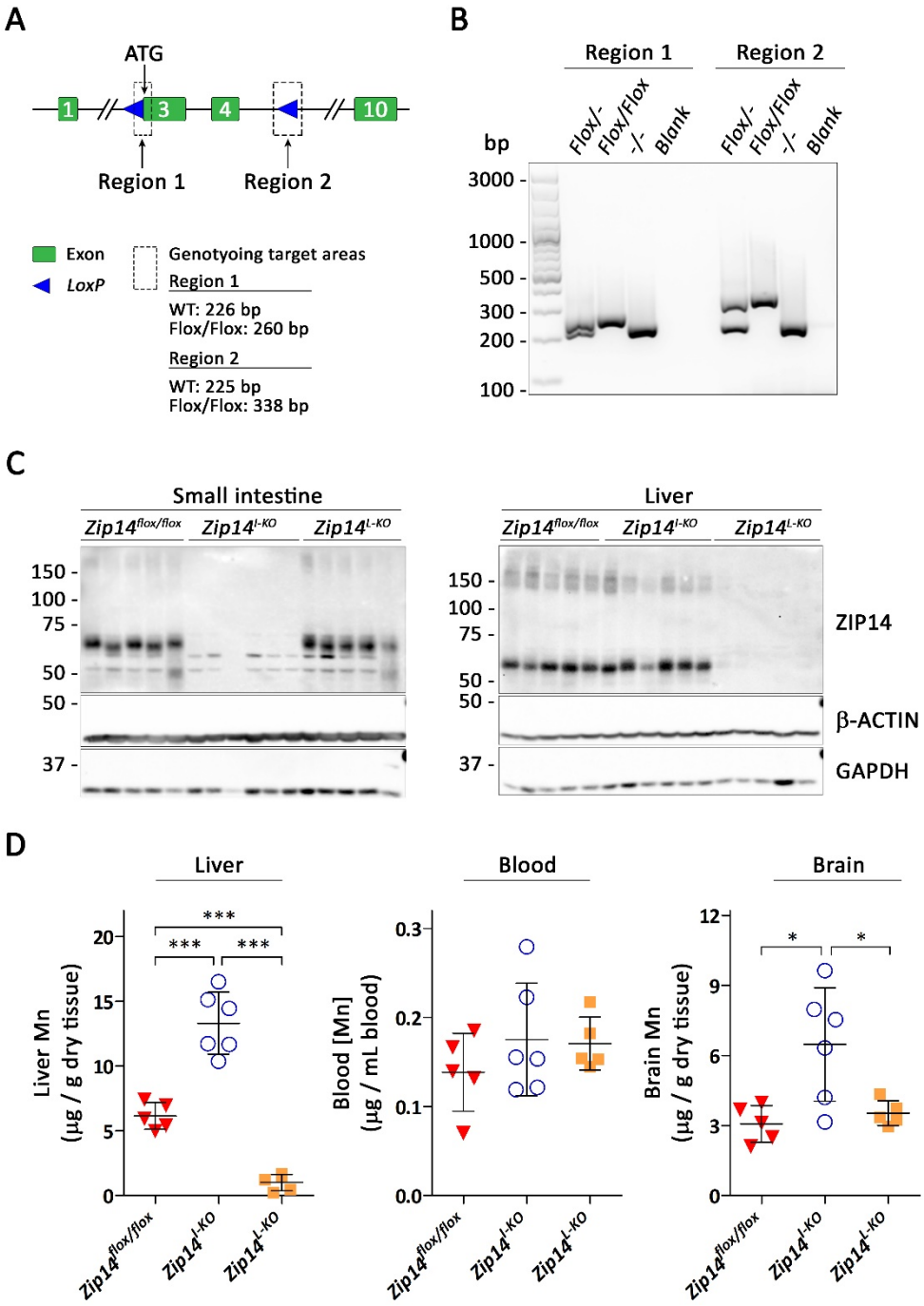

Figure 7: Intestine-specific deletion of *Zip14* in mice leads to Mn overload. (A) Gene targeting strategy for generating mice carrying *Zip14* conditional alleles. (B) Genotyping results using DNA isolated from heterozygous (Flox/-), homozygous (Flox/Flox) and wild-type (-/-) mice. (C) ZIP14 immunoblot of small intestine and liver samples from *Zip14*$^{flox/flox}$ (n=5, 3 male and 2 female), intestine-specific (*Zip14*$^{I\text{-}KO}$, n=6, 3 male and 3 female) and liver-specific (*Zip14*$^{L\text{-}KO}$, n=5, 3 male and 2 female) *Zip14* KO mice. Both β-ACTIN and GAPDH were used as loading controls. (D) Levels of Mn in livers, blood and brains of three-week-old *Zip14*$^{flox/flox}$, *Zip14*$^{I\text{-}KO}$ and *Zip14*$^{L\text{-}KO}$ mice. Statistical analysis was performed using one-way ANOVA followed by the Bonferroni post-hoc test with *$p < 0.05$ and ***$p < 0.001$.

Supporting Information

Intestinal ZIP14 is required for the control of systemic manganese homeostasis

Ivo Florin Scheiber, Yuze Wu, Shannon Elizabeth Morgan and Ningning Zhao*

From the Department of Nutritional Sciences, The University of Arizona, Tucson, AZ 85721, USA

Running title: *ZIP14 knock-out enhances Mn absorption*

*To whom correspondence should be addressed: Ningning Zhao, Department of Nutritional Sciences, The University of Arizona, Tucson, AZ 85721, USA. Tel.: (520) 621-9744; Fax: (520) 621-9446; Email: zhaonn@email.arizona.edu.

List of materials included: Supplemental Figures S1-S8

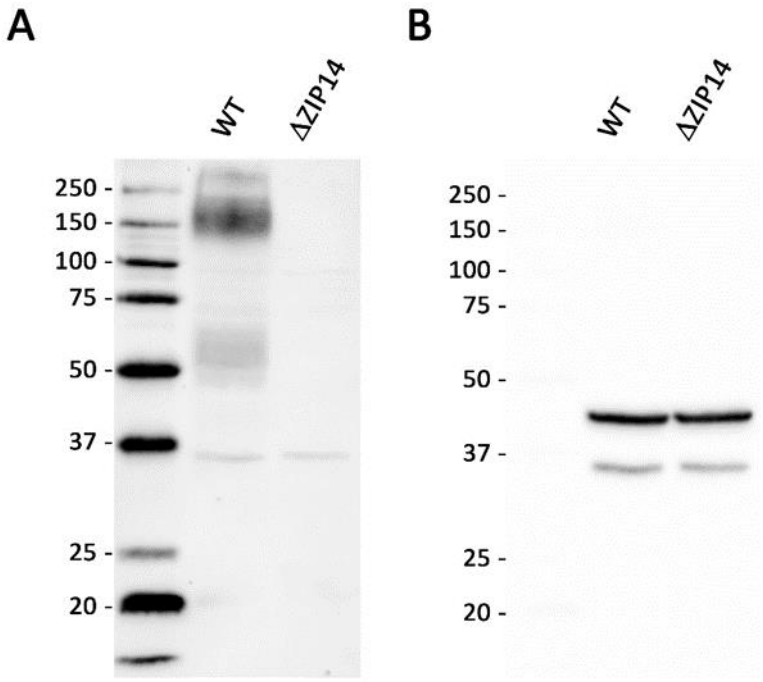

Figure S1. Uncropped immunoblots for Fig. 1D. Whole blots for (A) ZIP14, (B) β-ACTIN and GAPDH.

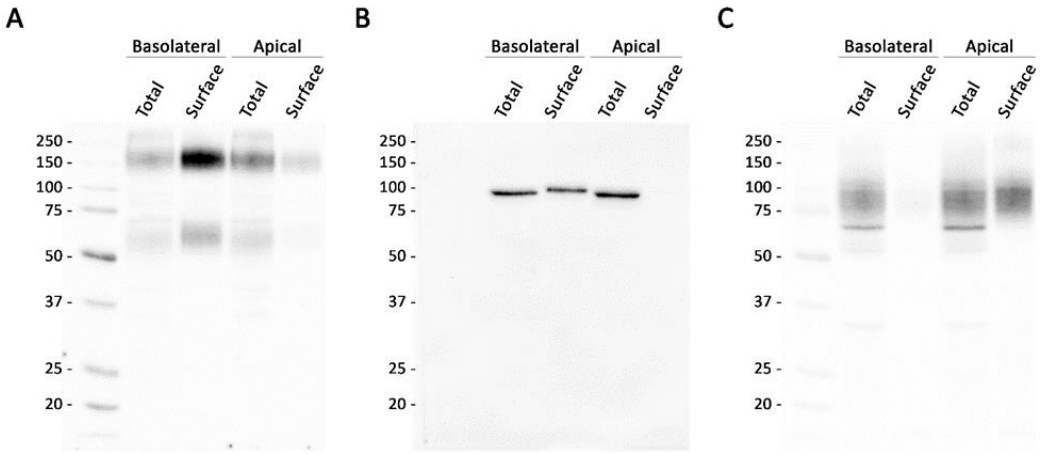

Figure S2. Uncropped immunoblots for Fig. 2E. Whole blots for (A) ZIP14, (B) Na^+K^+-ATPase and (C) DMT1.

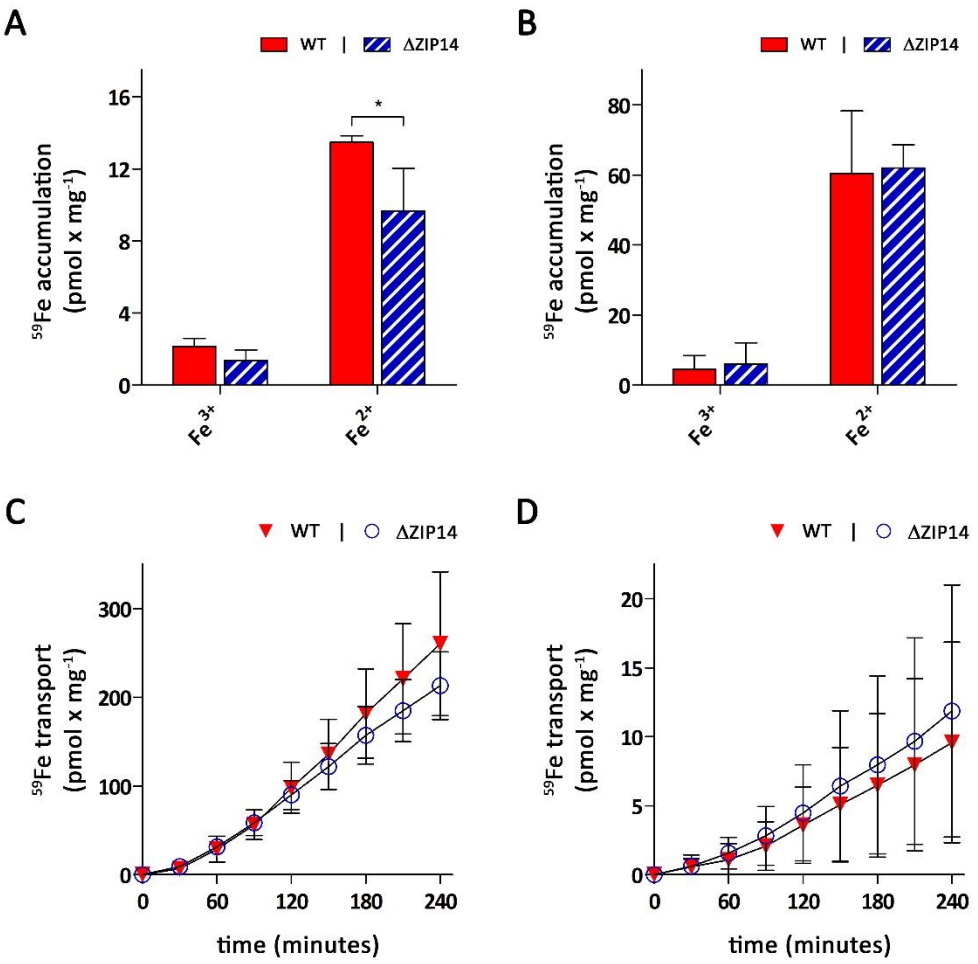

Figure S3. Fe accumulation and Fe transport by CaCo-2_{WT} and CaCo-$2_{\Delta ZIP14}$ monolayers. CaCo-2_{WT} (WT) and CaCo-$2_{\Delta ZIP14}$ (ΔZIP14) monolayers were incubated for 5 minutes with either 1 μM Fe(II)-ascorbate or Fe(III)-citrate spiked with 0.1 μM ^{59}Fe added to the (A) basolateral or (B) apical compartment to examine iron uptake. Apical-to-basolateral Fe transport experiments were initiated by adding either 1 μM (C) Fe(II)-ascorbate or (D) Fe(III)-citrate spiked with 0.1 μM ^{59}Fe to the apical compartment of CaCo-2_{WT} (WT) and CaCo-$2_{\Delta ZIP14}$ (ΔZIP14) monolayers and samples were collected every 30 minutes from the basolateral compartment and analyzed by γ-counting. During the accumulation and transport experiments the extracellular pH was maintained at pH 7.4 in the basolateral and pH 6.1 in the apical compartment. Data are presented as means ± s.d. from three independent experiments performed in duplicates. Statistical analysis was performed using two-way ANOVA followed by the Bonferroni post-hoc test with *$p < 0.05$.

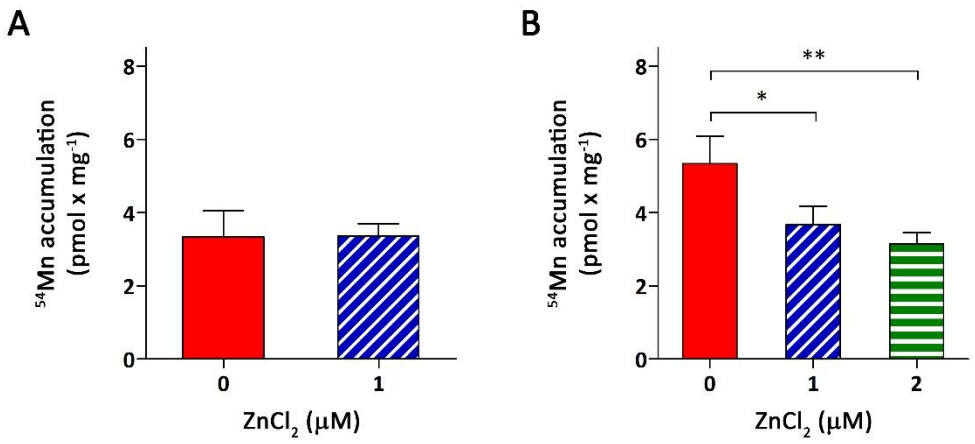

Figure S4. Zn competition for basolateral Mn-uptake by CaCo-2_{WT} monolayers. The cells were incubated for five minutes with 0.1 µM ^{54}Mn-citrate and either 0, 1 or 2 µM $ZnCl_2$ added to the basolateral compartment. Zn-competition experiments were carried out using either (A) transport medium (DMEM containing 1 mM pyruvate supplemented with 20 mM PIPES) or (B) salt-based incubation buffer as the basolateral medium. Transport medium was used as the apical medium. During the experiments the extracellular pH was maintained at 7.4 in the basolateral and pH 6.1 in the apical compartment. Data are presented as means ± s.d. from (A) five or (B) three independent experiments. Statistical analysis was performed using Student's t-test with*$p < 0.05$ and **$p < 0.01$.

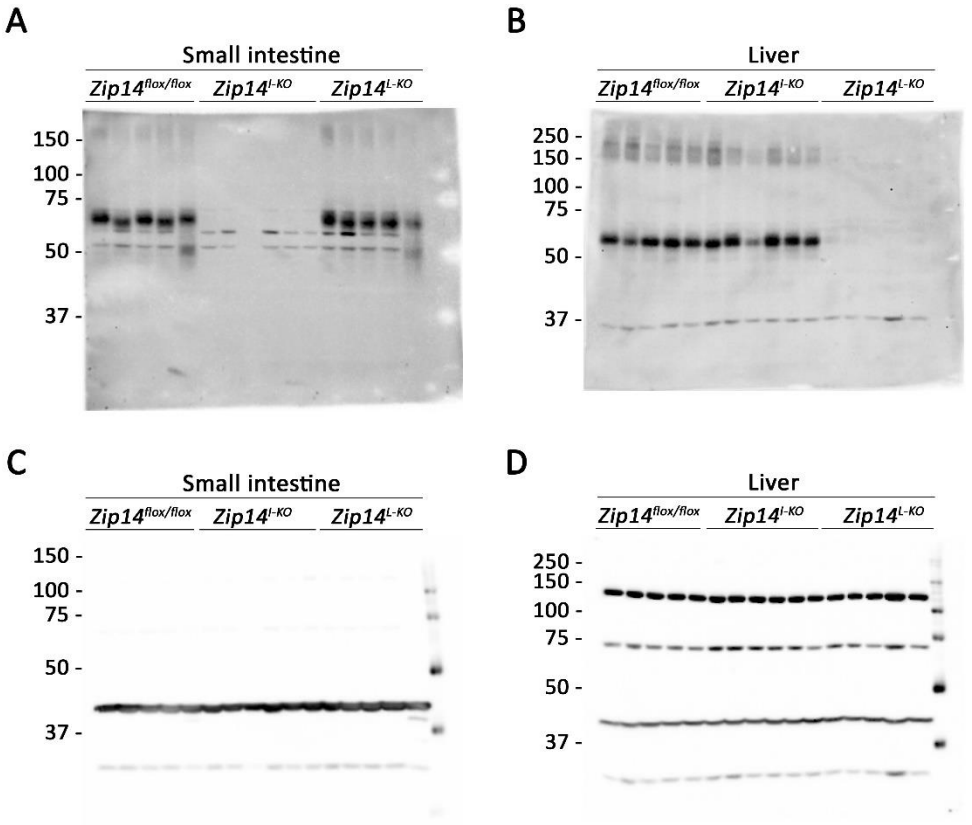

Figure S5. Uncropped immunoblots for Fig. 7C. Whole blots for (A, B) ZIP14 and (C, D) β-ACTIN and GAPDH

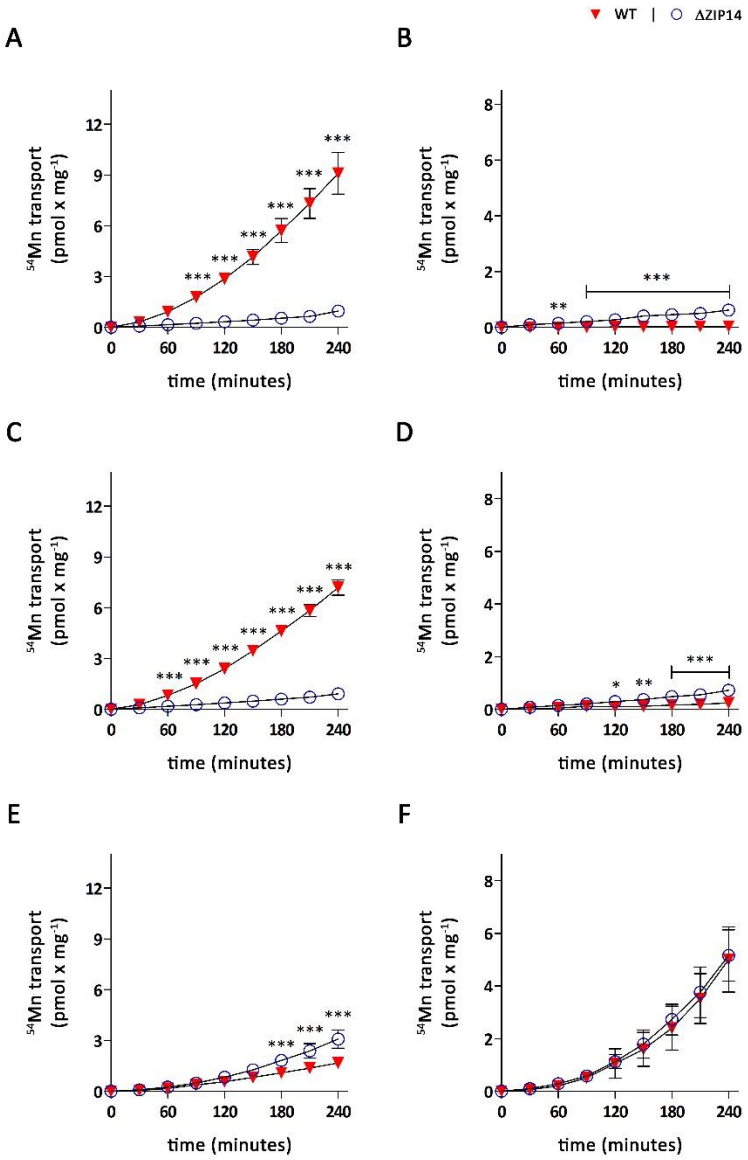

Figure S6. pH-dependent Mn transport by CaCo-2_{WT} (WT) and CaCo-$2_{\Delta ZIP14}$ (ΔZIP14) monolayers. Mn-transport experiments were initiated by adding 0.1 μM ^{54}Mn-citrate either to the (A, C, E) basolateral or (B, D, F) apical compartment of WT and ΔZIP14 monolayers. Samples were collected every 30 min from the opposite compartment and analyzed by γ-counting. During the transport experiments the extracellular pH was maintained at (A, B) 7.4, (C, D) 6.8 or (E, F) 6.1 in both the basolateral and apical compartment. Data are presented as means ± s.d. from three independent experiments performed in duplicates. Statistical analysis was performed using two-way ANOVA followed by the Bonferroni post-hoc test with *$p < 0.05$, **$p < 0.01$ and ***$p < 0.001$. The horizontal bars indicate same significant levels.

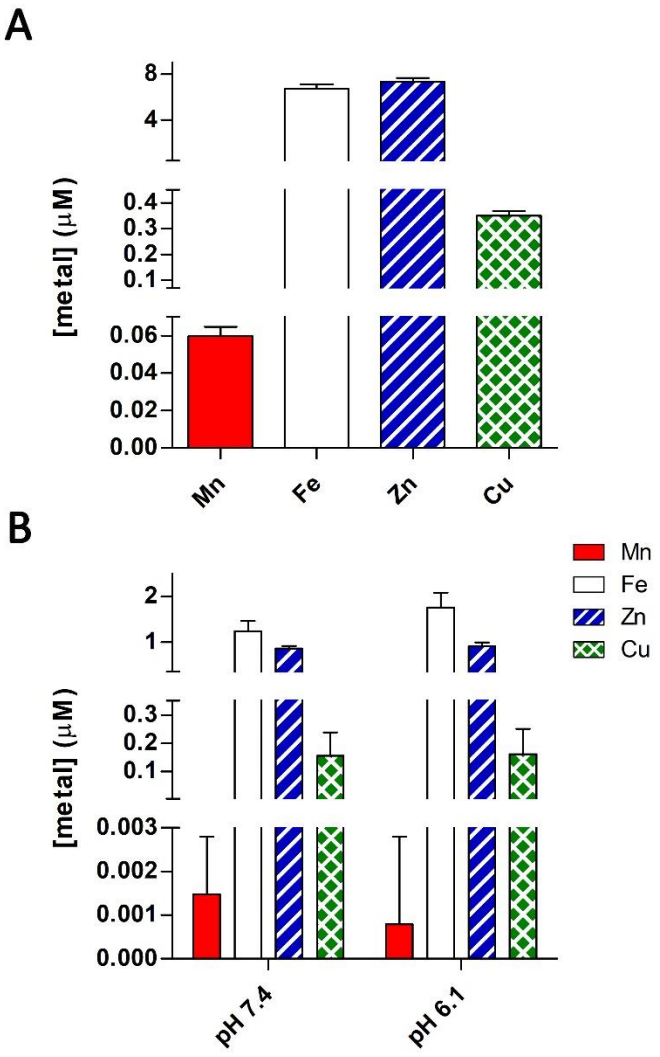

Figure S7. Concentrations of Mn, Fe, Zn and Cu in (A) growth medium (80% Dulbecco's modified Eagles medium (DMEM) containing 1 mM pyruvate supplemented with 3.7 g/L $NaHCO_3$, 1x non-essential amino acids, 100 units x mL^{-1} penicillin, 100 μg x mL^{-1} streptomycin, and 20% fetal bovine serum and (B) transport medium (DMEM containing 1 mM pyruvate supplemented with 20 mM PIPES) adjusted to either pH 7.4 or pH 6.1. Metal concentrations in the media were determined by inductively coupled plasma mass spectrometry at the Arizona Laboratory for Emerging Contaminants (ALEC), Tucson, AZ, USA. Data are presented as means ± s.d. from three independent experiments.

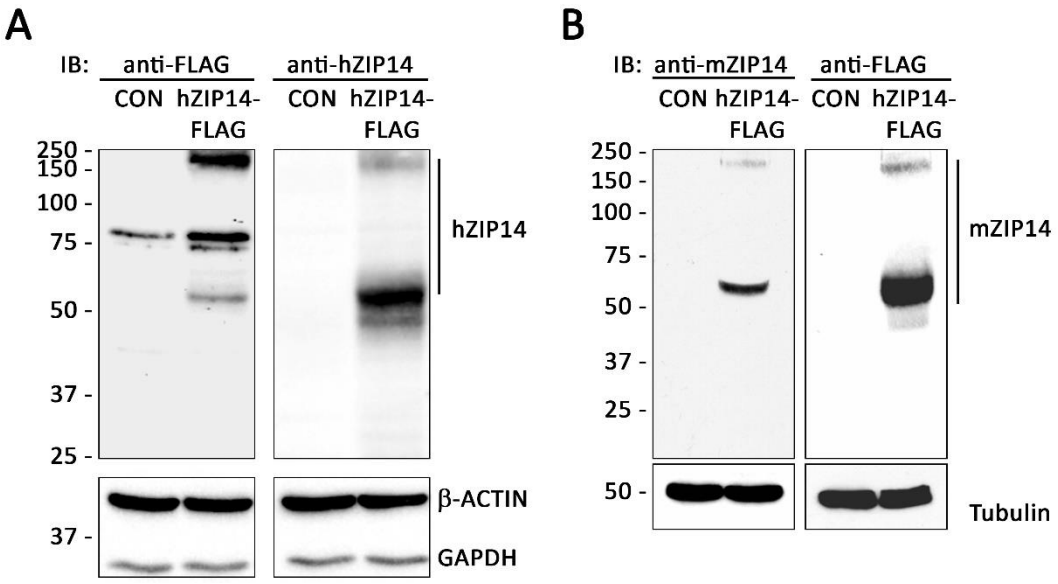

Figure S8. To confirm the specificity of (A) anti-hZIP14 and (B) mZIP14 antibodies, we transfected HEK293 cells with an empty vector (CON), a vector encoding hZIP14 with a FLAG epitope (hZIP14-FLAG), or a vector encoding mZIP14 with a FLAG epitope (mZIP14-FLAG). Cells were lysed 48 hours after transfection and lysates were analyzed by immunoblotting (IB) with anti-FLAG, anti-hZIP14 or anti-mZIP14 antibodies. The predicted molecular weights of hZIP14 and mZIP14 are 54 kDa, the immunoreactive band around 150 kDa represents a multimeric form of hZIP14. Our anti-hZIP14 and anti mZIP14 antibodies detect both monomeric and multimeric forms of ZIP14. (A) β-ACTIN and GAPDH or (B) Tubulin were used as loading controls.